Influence of spatial and dynamical anisotropies on flow and femtoscopy radii in relativistic heavy-ion collisions at LHC

E. Zabrodin,

in collaboration with

L. Bravina, I. Lokhtin, L. Malinina, S. Petrushanko and A. Snigirev

ICNFP-2018, OAC, Kolymbari, Crete, Greece, 4.07. – 12.07.2018

Outline

I. HYDJET++ model
II. Description of elliptic and triangular flow in relativistic heavy-ion collisions
III. Anisotropic flow e-by-e fluctuations
IV. Femtoscopic correlations
V. Geometric and dynamical anisotropy
VI. Flow and oscillations of the femtoscopic radii (simultaneous description)
VII. Conclusions

I. HYDJET++ = FASTMC + HYDJET

Dynamic Regimes

Parton distribution,
Nuclear geometry
Nuclear shadowing

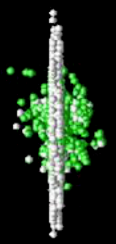

Parton production &
regeneration
(or, sQGP)

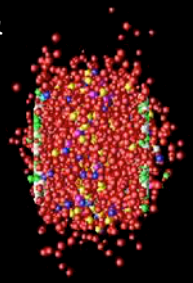

Chemical freeze-out
(Quark recombination)

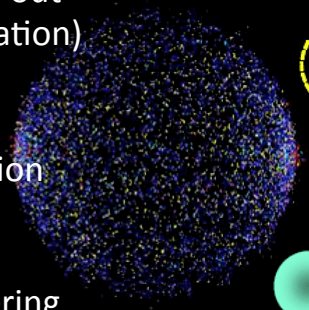

Jet fragmentation
functions

Hadron rescattering

Thermal freeze-out

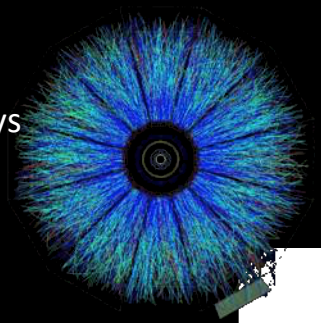

Hadron decays

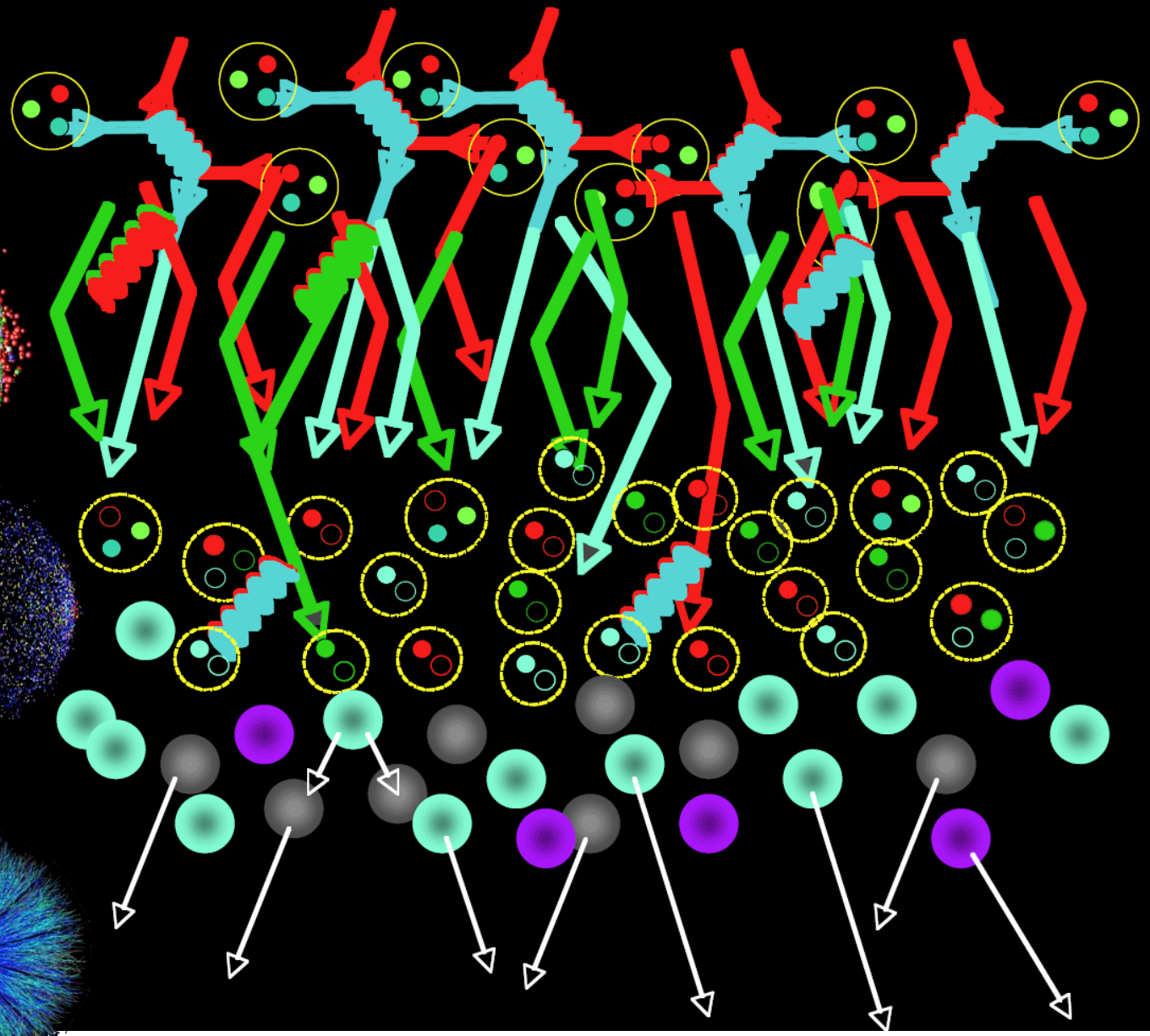

Diagram by Peter Steinberg

HYDJET++ model for heavy ion collisions

Simplifies the pictures of heavy ion collisions as merging of 2 components:

(as independent parts)

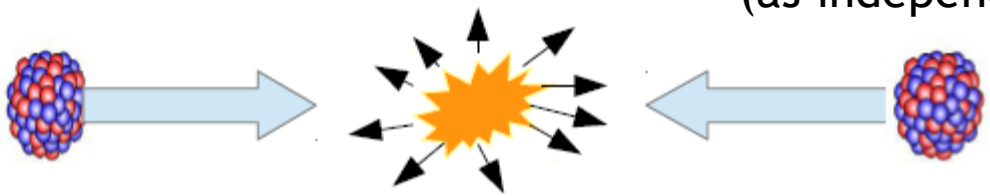

- soft hydro-type part

(represented by hadron emission assuming thermal equilibrium)

Based on the adapted FAST MC model:

N.S.Amelin, R.Lednisky, T.A.Pocheptsov, I.P.Lokhtin, L.V.Malinina, A.M.Snigirev, Yu.A.Karpenko, Yu.M.Sinyukov, *Phys. Rev. C 74 (2006) 064901*

N.S.Amelin, R.Lednisky, I.P.Lokhtin, L.V.Malinina, A.M.Snigirev, Yu.A.Karpenko, Yu.M.Sinyukov, I.C.Arsene, L.Bravina, *Phys. Rev. C 77 (2008) 014903*

HYDJET++ (soft): main physics assumptions

A hydrodynamic expansion of the fireball is supposed to end by a sudden system breakup at given T and chemical potentials. Momentum distribution of produced hadrons keeps the thermal character of the equilibrium distribution.

Cooper-Frye formula: $$p^0 \frac{d^3N_i}{d^3p} = \int_{\sigma(x)} d^3\sigma_\mu(x)\, p^\mu\, f_i^{eq}(p^\nu u_\mu(x); T, \mu_i)$$

- HYDJET++ avoids straightforward 6-dimensional integration by using the special simulation procedure (like HYDJET): momentum generation in the rest frame of fluid element, then Lorentz transformation in the global frame → uniform weights → effective von-Neumann rejection-acception procedure.

Freeze-out surface parameterizations

1. The Bjorken model with hypersurface $\tau = (t^2 - z^2)^{1/2} = const$
2. Linear transverse flow rapidity profile $\rho_u = \frac{r}{R}\rho_u^{\max}$
3. The total effective volume for particle production at

- $$V_{eff} = \int_{\sigma(x)} d^3\sigma_\mu(x) u^\mu(x) = \tau \int_0^R \gamma_r r dr \int_0^{2\pi} d\phi \int_{\eta_{\min}}^{\eta_{\max}} d\eta = 2\pi\tau\Delta\eta \left(\frac{R}{\rho_u^{\max}}\right)^2 (\rho_u^{\max}\sinh\rho_u^{\max} - \cosh\rho_u^{\max} + 1)$$

HYDJET++ model for heavy ion collisions

Simplifies the pictures of heavy ion collisions as merging of 2 components:

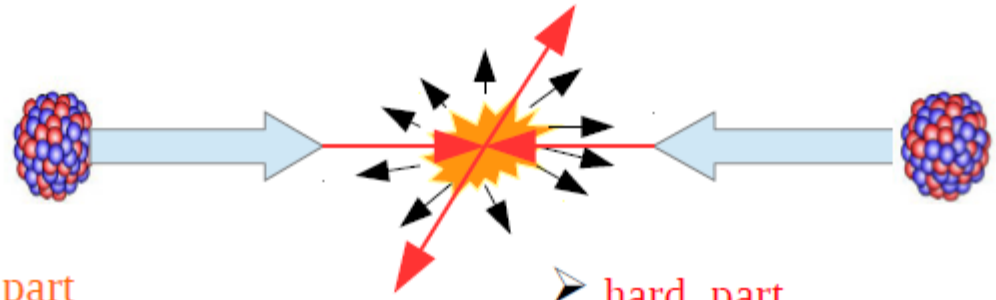

- soft hydro-type part
  (represented by hadron emission assuming thermal equilibrium)

- hard part
  (represented by hard parton scattering and later hadronization)

Based on PYTHIA with quenching:
PYQUEN: I.P.Lokhtin, A.M.Snigirev,
Eur. Phys. J. 45 (2006) 211

Nuclear shadowing is accounted for:
K.Tywoniuk et al., Phys. Lett. B 657 (2007) 170)

http://cern.ch/lokhtin/hydjet++

(latest version 2.3)

I.Lokhtin, L.Malinina, S.Petrushanko, A.Snigirev, I.Arsene, K.Tywoniuk,
Comp.Phys.Comm. 180 (2009) 779

HYDJET++ model for heavy ion collisions

Simplifies the pictures of heavy ion collisions as merging of 2 components:

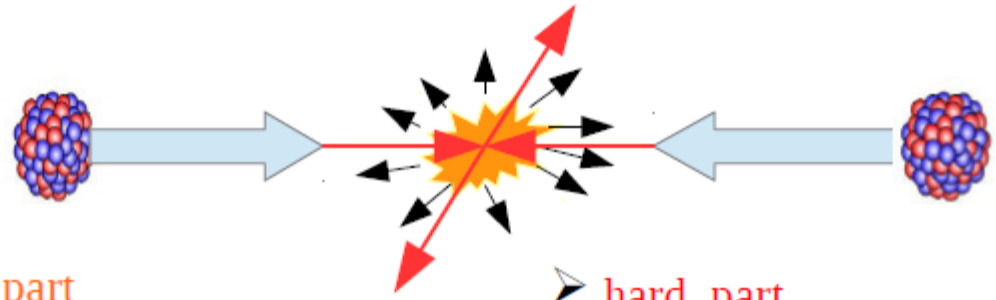

- soft hydro-type part
(represented by hadron emission assuming thermal equilibrium)

- hard part
(represented by hard parton scattering and later hadronization based on PYTHIA)

Soft and hard components:

- The contribution of the hard part to the total multiplicity is control by p_{Tmin} parameter (parton hard scattering in PYTHIA)
- Modification of the hard part due to interactions with the medium is simulated
- No modification of soft part

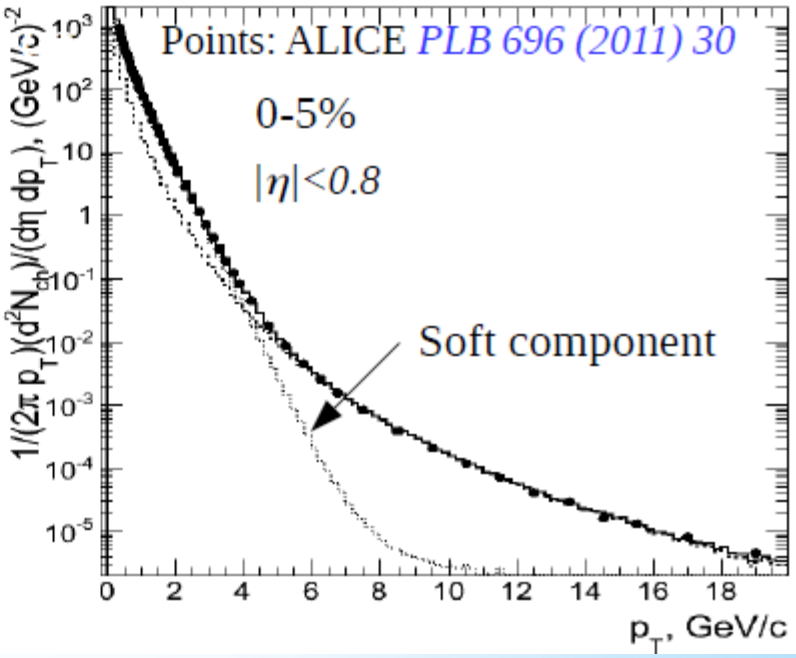

Hard component

Initial parton configuration
PYTHIA w/o hadronization

→ **parton rescattering & energy loss**

→ **Hadronization**
PYTHIA w hadronization

Energy loss, general kinetic integral equation with scattering probability density:

$$\triangle E(L,E) = \int_0^L dl \frac{dP(l)}{dl} \lambda(l) \frac{dE(l,E)}{dl} \qquad \frac{dP(l)}{dl} = \frac{1}{\lambda(l)} \exp(-l/\lambda(l))$$

- Collisional loss
(high momentum transfer approximation)

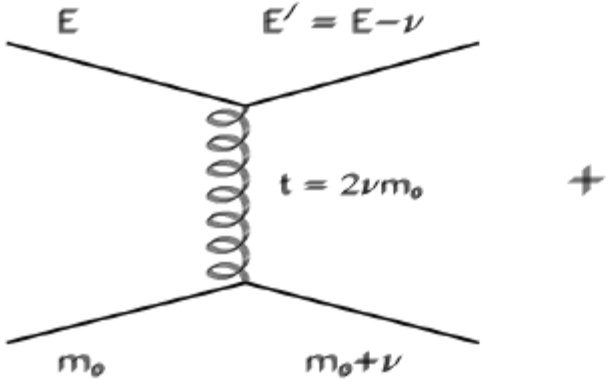

+

- Radiative loss (coherent gluon radiation in Baier-Dokshitzer-Mueller-Schiff formalism)

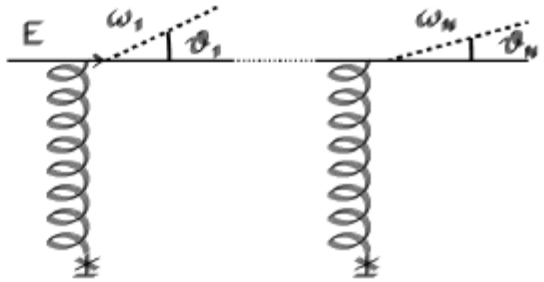

- "Dead" cone approximation for massive quarks

Charged multiplicity vs centrality and pseudorapidity in HYDJET++ at LHC

I.P. Lokhtin, A.V. Belyaev, L.V. Malinina, S.V. Petrushanko, E.P. Rogochaya, A.M. Snigirev, Eur.Phys.J. C (2012) 72:2045

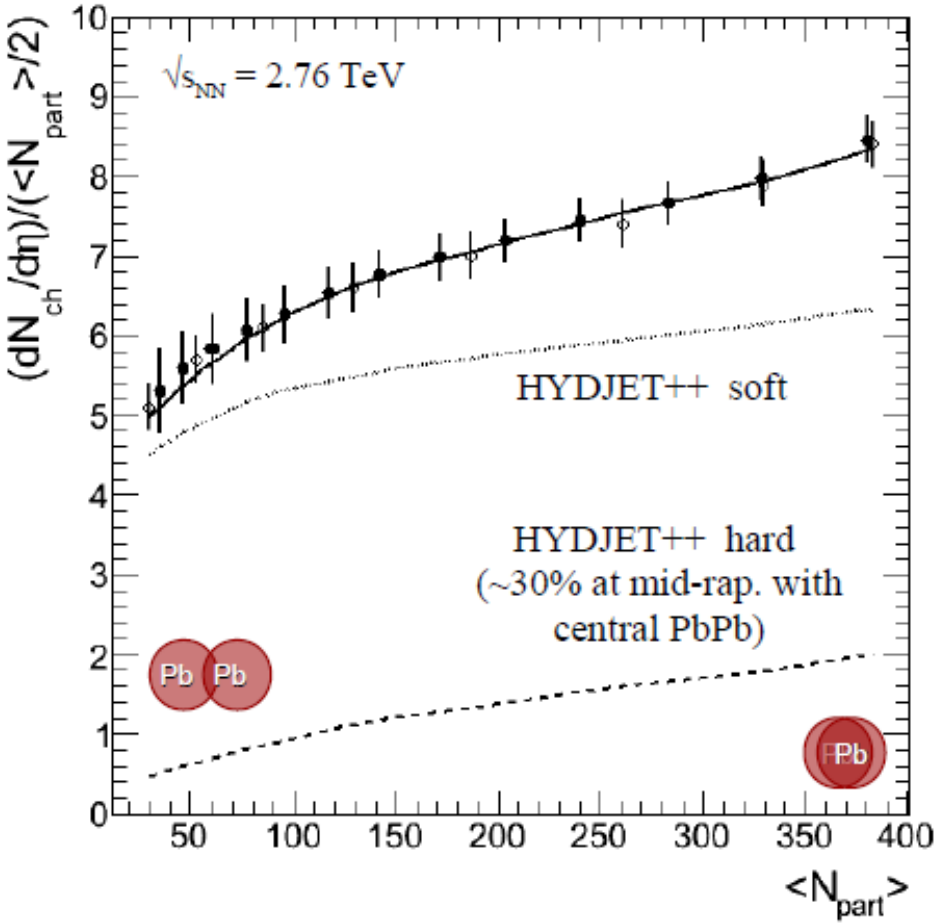

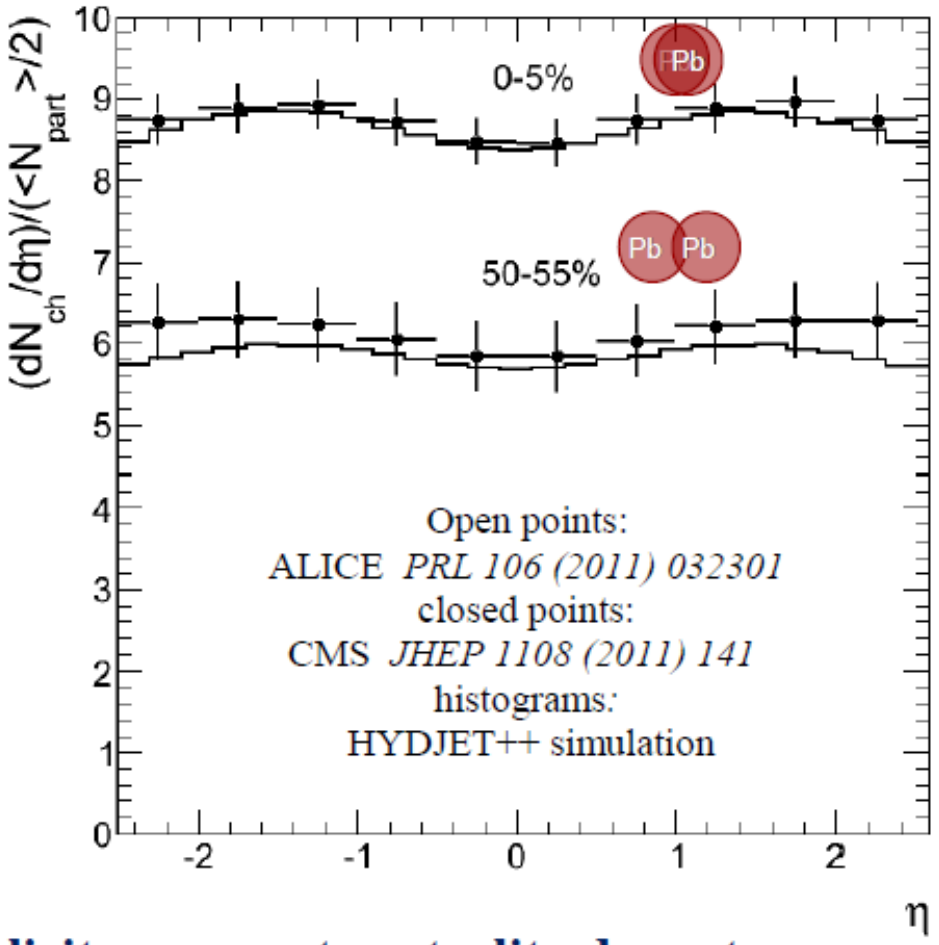

Tuned HYDJET++ reproduces multiplicity vs. event centrality down to very peripheral events, as well as approximately flat pseudorapidity distribution.

P_T spectrum and R_{AA} factor for charged hadrons in HYDJET++ at LHC

I.P. Lokhtin, A.V. Belyaev, L.V. Malinina, S.V. Petrushanko, E.P. Rogochaya, A.M. Snigirev, Eur.Phys.J. C (2012) 72:2045

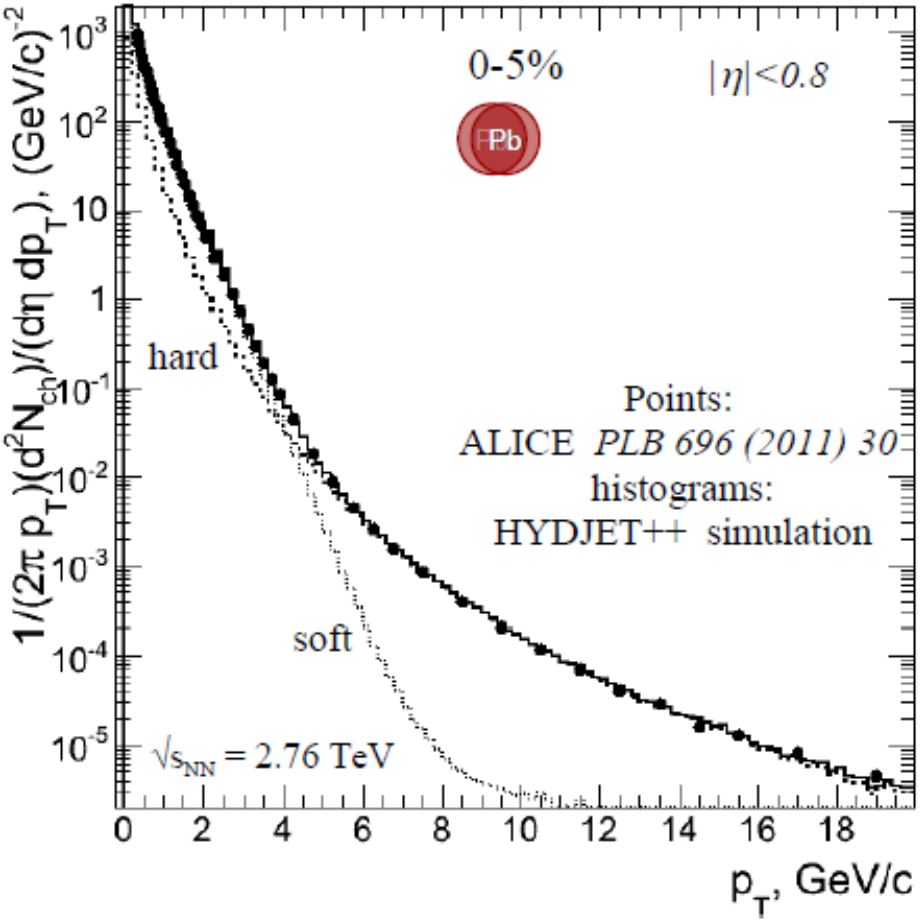

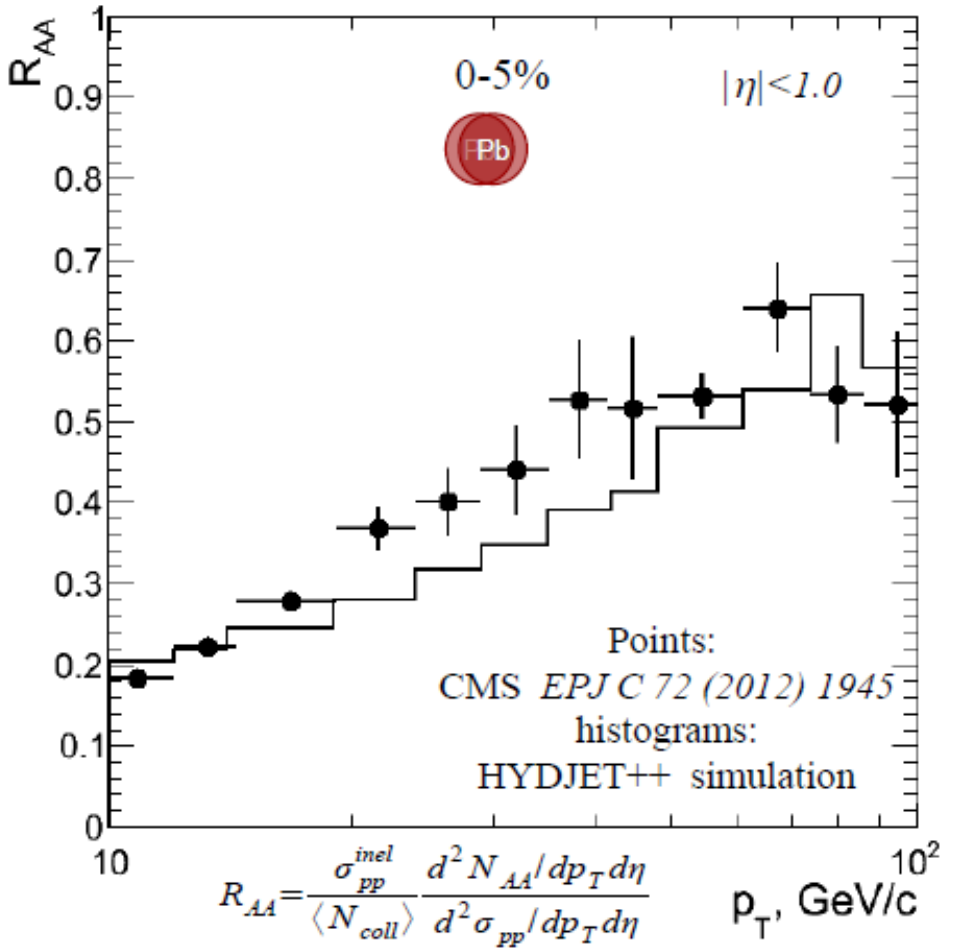

HYDJET++ reproduces p_T-spectrum and R_{AA} for central PbPb collisions in mid-rapidity up to $p_T \sim 100$ GeV/c .

II. Elliptic and Triangular flow in HYDJET++ : interplay of hydrodynamics and jets

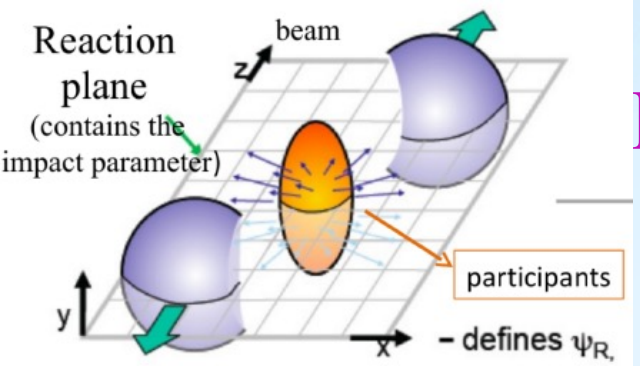

ELLIPTIC FLOW

Initial spatial anisotropy is converted to anisotropy in momentum space

Initial anisotropy

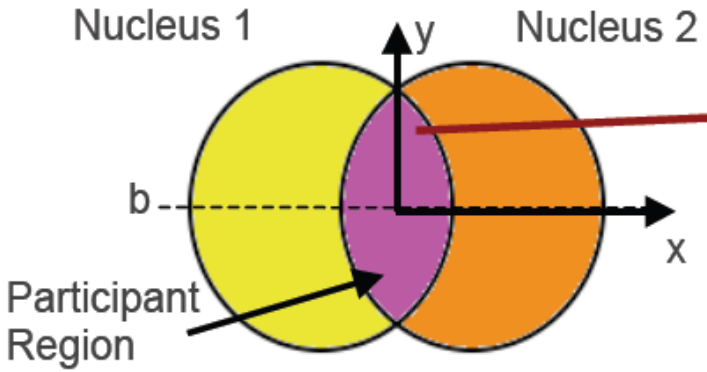

Pressure driven expansion

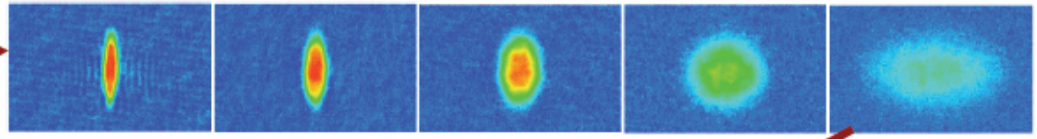

Final anisotropy

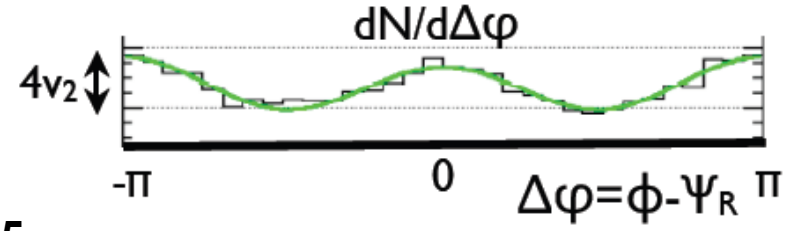

$$\frac{dN}{d\phi} = \frac{N}{2\pi}\left(1 + \sum 2v_n \cos\left(n(\phi - \psi_R)\right)\right)$$

S.Voloshin, Y.Zhang, Z.Phys.C70 (1996) 665

$$v_2 = \left\langle \cos\left(2(\phi - \psi_R)\right)\right\rangle \propto \varepsilon$$

Elliptic flow is quantified by the second Fourier coefficient (v_2) of the observed particle distribution

TRIANGULAR FLOW

B. Alver and G.Roland, PRC 81 (2010) 054905

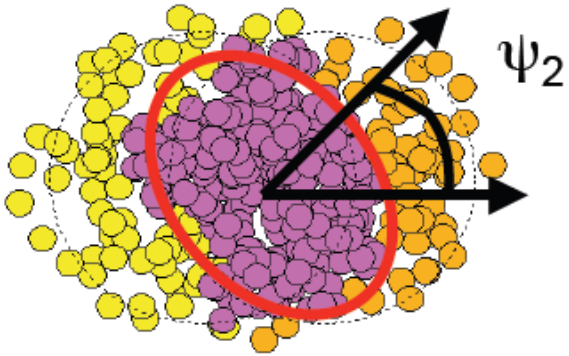

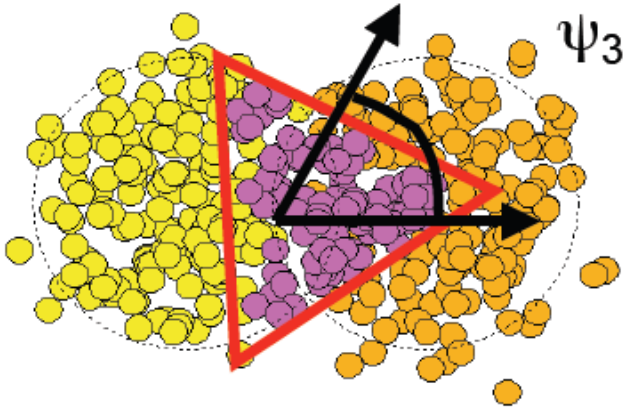

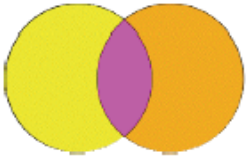

$$\frac{dN}{d\phi} = \frac{N}{2\pi}\left(1 + \sum 2v_n \cos\left(n(\phi - \psi_R)\right)\right)$$

$$v_2 = \left\langle \cos\left(2(\phi - \psi_R)\right)\right\rangle$$

$$v_3 = 0$$

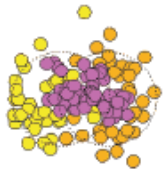

$$\frac{dN}{d\phi} = \frac{N}{2\pi}\left(1 + \sum 2v_n \cos\left(n(\phi - \psi_n)\right)\right)$$

$$v_2 = \left\langle \cos\left(2(\phi - \psi_2)\right)\right\rangle$$

$$v_3 = \left\langle \cos\left(3(\phi - \psi_3)\right)\right\rangle$$

The triangular initial shape leads to triangular hydrodynamic flow

Anisotropic flow generation in HYDJET++

Elliptic flow v_2

$$v_2 \propto \frac{2(\delta-\epsilon)}{(1-\delta^2)(1-\epsilon^2)}$$

- Spatial modulation of freeze-out surface;
- fluid velocity modulation.

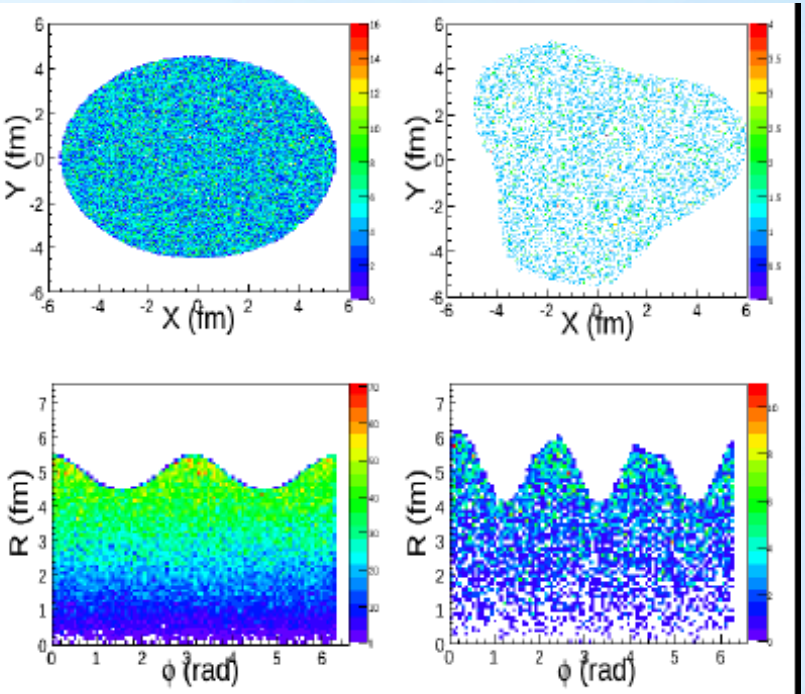

Spatial anisotropy

$$\varepsilon(b) = \frac{R^2_y - R^2_x}{R^2_y + R^2_x}$$

Momentum anisotropy

$$\tan\varphi_u = \sqrt{\frac{1-\delta(b)}{1+\delta(b)}}\tan\varphi$$

R(b) – surface radius

φ_u - azimuthal angle of fluid velocity

φ - spatial azimuthal angle

Triangular flow v_3

Spatial anisotropy

$$R(b,\phi) = R_{ell}(b,\phi)\{1+\epsilon_3(b)\cos[3(\phi-\Psi_3)]\}, \qquad R_{ell}(b,\phi) = R_{fo}(b)\frac{\sqrt{1-\epsilon^2(b)}}{\sqrt{1+\epsilon(b)\cos 2\phi}}.$$

Momentum anisotropy

$$\rho_u^{max}(b) = \rho_u^{max}(0)\{1+\rho_3(b)\cos[3(\phi-\Psi_{EP,3})]+\ldots\}$$

Four parameters ε, ε_3, δ, ρ_3 are tuned to fit experimental data

LHC data vs. HYDJET++ model

Elliptic flow

Pb+Pb @ 2.76 ATeV

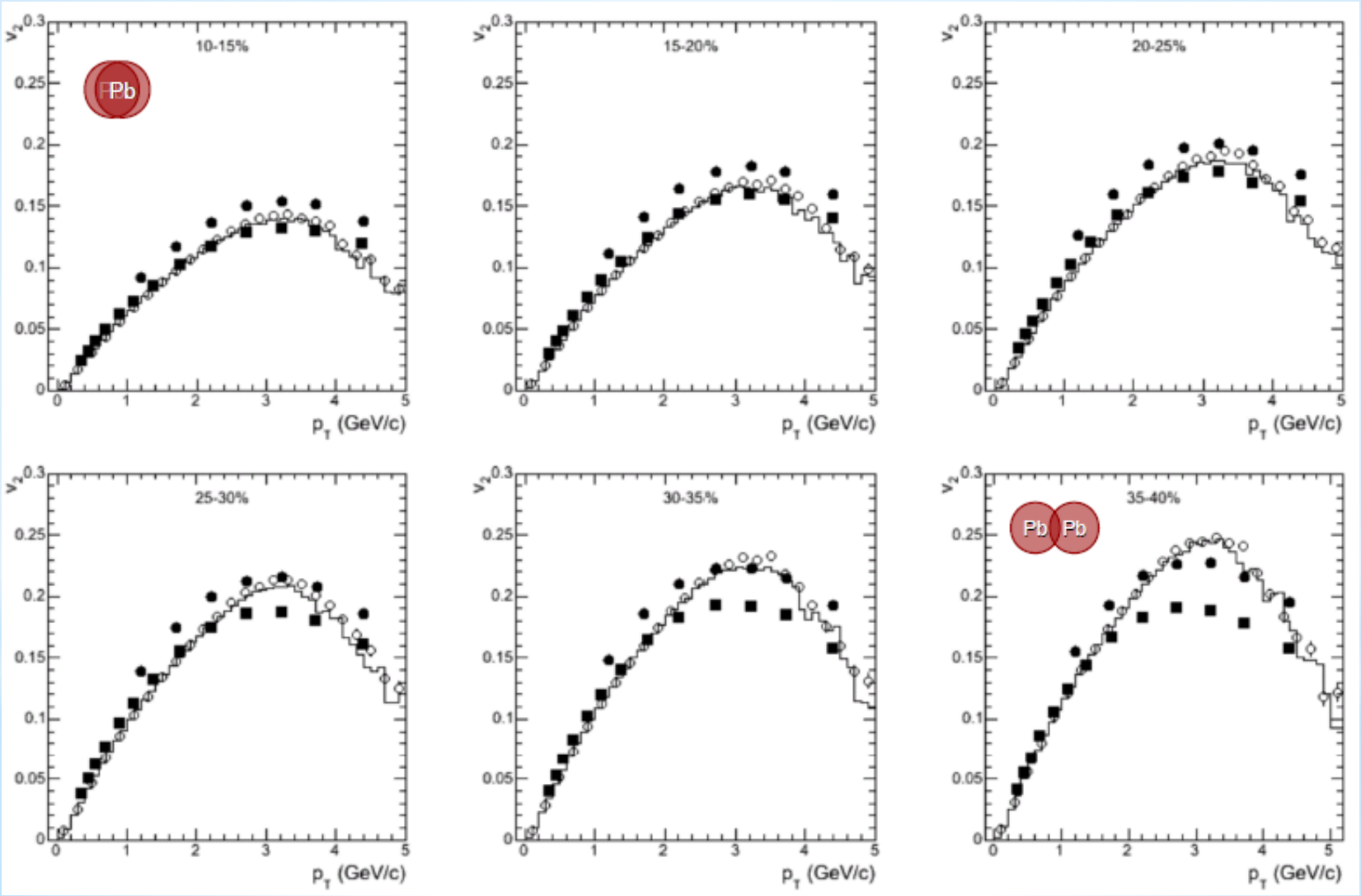

Closed points: CMS data v_2{2Part & LYZ};
Open points and histograms: HYDJET++ v_2{EP & Psi2}

L. Bravina et al., Eur. Phys. J C74 (2014) 2807

LHC data vs. HYDJET++ model

Triangular flow

Pb+Pb @ 2.76 ATeV

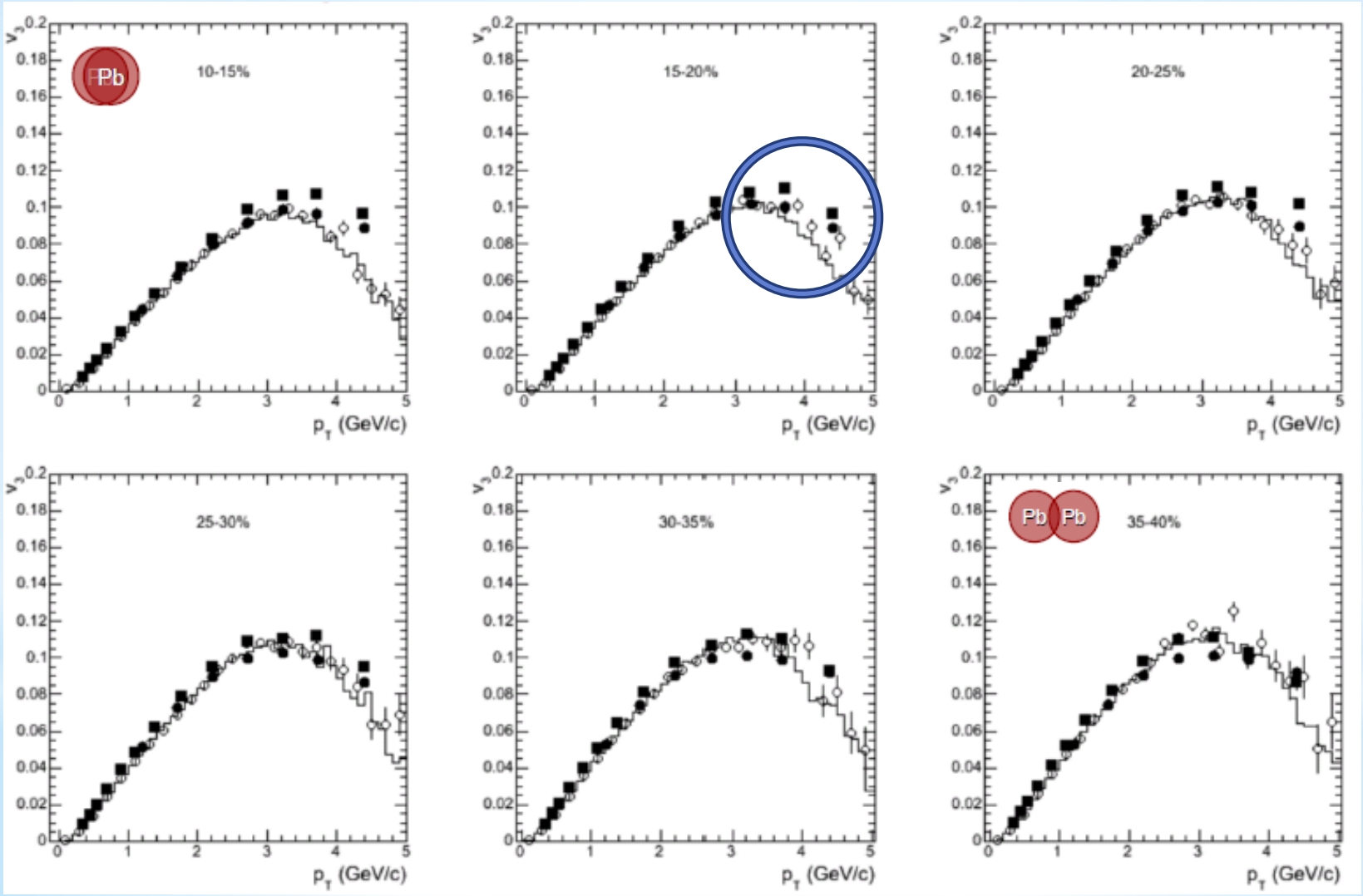

L. Bravina et al., Eur. Phys. J. C74 (2014) 2807

Closed points: CMS data v_3{2Part & LYZ};
Open points and histograms: HYDJET++ v_3{EP & Psi3}

Interplay of hydrodynamics and jets

Triangular flow

Pb+Pb @ 2.76 ATeV

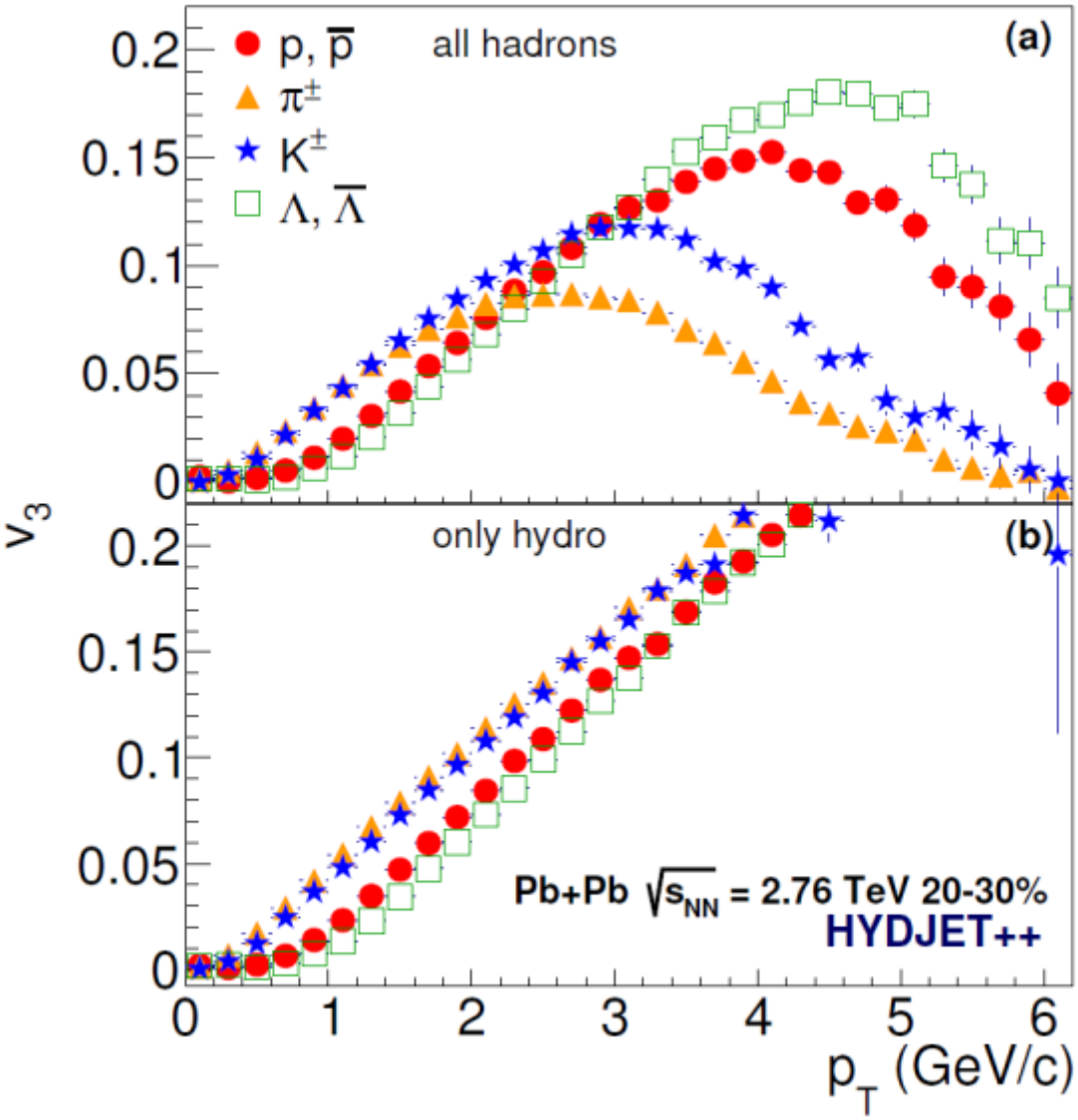

Hydrodynamics gives mass ordering of v_3

The model possesses crossing of baryon and meson branches

The reason for the mass ordering break at 2 GeV/c is traced to hard processes (jets)

III. Anisotropic flow E-by-E fluctuations

Intrinsic fluctuations in HYDJET++

Event-by-event flow vector V_n

Pb+Pb @ 2.76 ATeV

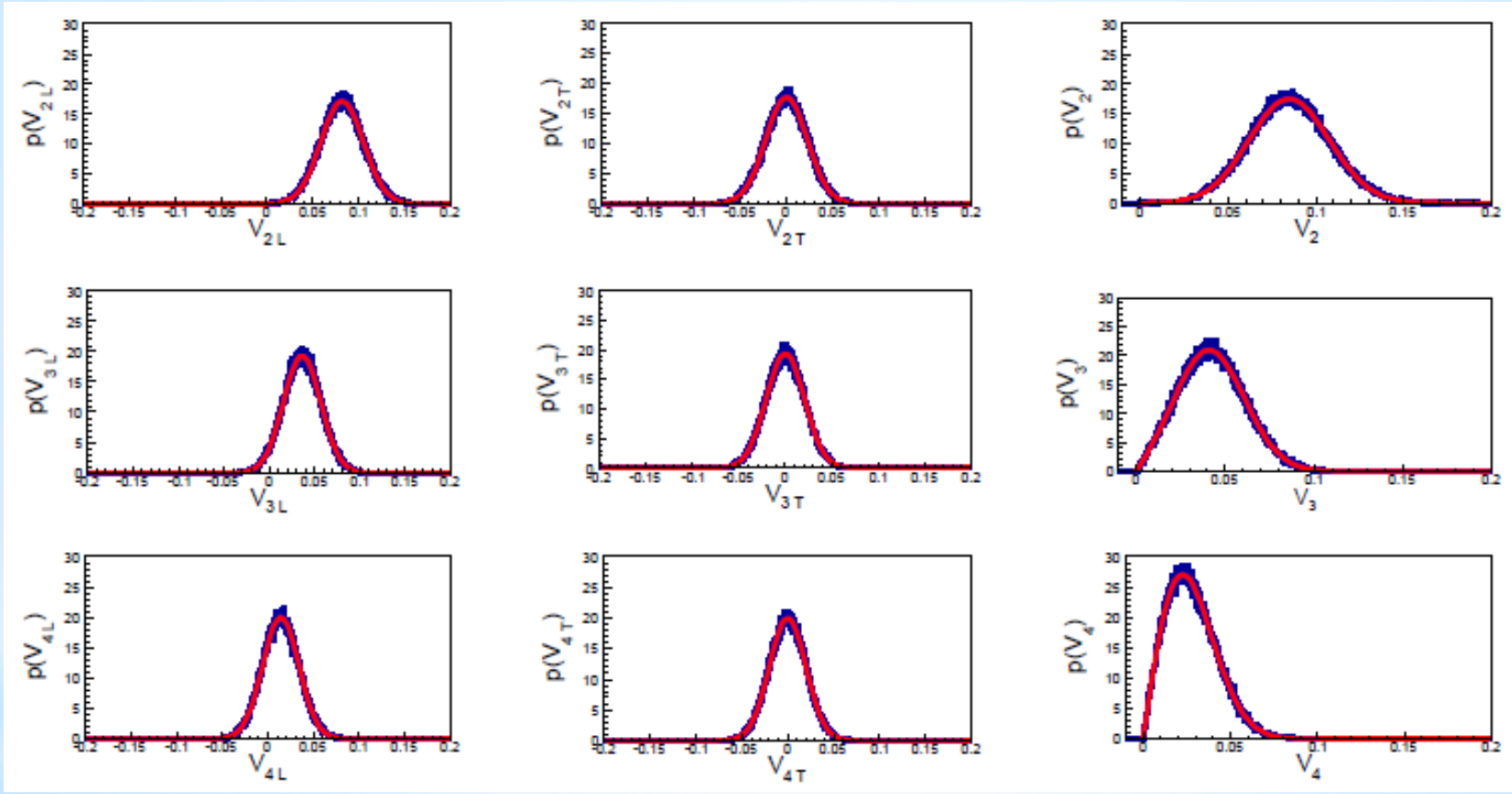

L. Bravina et al., EPJC 75 (2015) 588

$$p(V_{\mathrm{nL}}) = \frac{1}{\sqrt{2\pi\sigma_n^2(b)}} \exp\left[-\frac{(V_{\mathrm{nL}} - \langle V_{\mathrm{nL}}\rangle)^2}{2\sigma_n^2(b)}\right] \qquad p(V_{\mathrm{nT}}) = \frac{1}{\sqrt{2\pi\sigma_n^2(b)}} \exp\left[-\frac{(V_{\mathrm{nT}})^2}{2\sigma_n^2(b)}\right]$$

Centrality = 20-25%

$$p(V_n) = \frac{V_n}{\sigma_n^2(b)} \exp\left[-\frac{V_n^2 + \langle V_{\mathrm{nL}}\rangle^2}{2\sigma_n^2(b)}\right] I_0\left(\frac{V_n \langle V_{\mathrm{nL}}\rangle}{\sigma_n^2(b)}\right)$$

S.Voloshin et al., PLB 659 (2008) 537; R.Bhalerao, J.-Y. Ollitrault, PLB 641 (2006) 260

Bayesian unfolding procedure

$$\frac{dN}{d\varphi} \propto 1 + 2\sum_{n=1}^{\infty} V_{\mathrm{n}}^{\mathrm{obs}} \cos\left[n(\varphi - \Psi_{\mathrm{n}}^{\mathrm{obs}})\right] =$$
$$= 1 + 2\sum_{n=1}^{\infty} (V_{\mathrm{n,x}}^{\mathrm{obs}} \cos n\varphi + V_{\mathrm{n,y}}^{\mathrm{obs}} \sin n\varphi)$$

$$V_{\mathrm{n}}^{\mathrm{obs}} = \sqrt{(V_{\mathrm{n,x}}^{\mathrm{obs}})^2 + (V_{\mathrm{n,y}}^{\mathrm{obs}})^2}\ ,$$
$$V_{\mathrm{n,x}}^{\mathrm{obs}} = V_{\mathrm{n}}^{\mathrm{obs}} \cos n\Psi_{\mathrm{n}}^{\mathrm{obs}} = \langle \cos n\varphi \rangle$$
$$V_{\mathrm{n,y}}^{\mathrm{obs}} = V_{\mathrm{n}}^{\mathrm{obs}} \sin n\Psi_{\mathrm{n}}^{\mathrm{obs}} = \langle \sin n\varphi \rangle\ .$$

Response function

$$p(V_{\mathrm{n}}^{\mathrm{obs}}|V_{\mathrm{n}}) \propto V_{\mathrm{n}}^{\mathrm{obs}} \exp\left[-\frac{(V_{\mathrm{n}}^{\mathrm{obs}})^2 + V_{\mathrm{n}}^2}{2\delta^2}\right] I_0\left(\frac{V_{\mathrm{n}}^{\mathrm{obs}} V_{\mathrm{n}}}{\delta^2}\right)$$

Unfolding matrix

$$M_{ij}^{\mathrm{iter}} = \frac{A_{ji} c_i^{\mathrm{iter}}}{\sum_{m,k} A_{mi} A_{jk} c_k^{\mathrm{iter}}},$$
$$\widehat{c}^{\,\mathrm{iter}+1} = \widehat{M}^{\mathrm{iter}} \widehat{e}, A_{ji} = p(e_j|c_i)$$

G.Aad et al. (ATLAS), JHEP 1311 (2013) 183

The method excludes the non-flow effects and extracts the genuine flow fluctuations

Fluctuations of elliptic flow in the model

Unsmeared parameter ε

Pb+Pb @ 2.76 ATeV

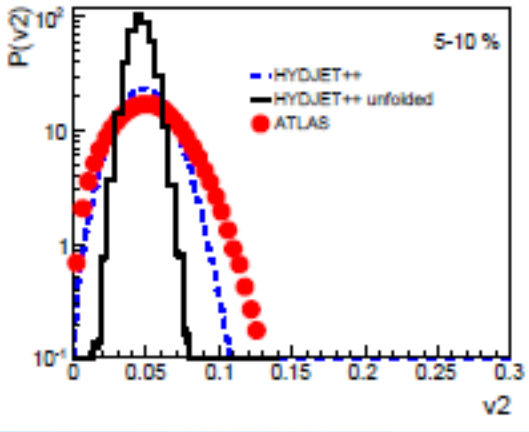

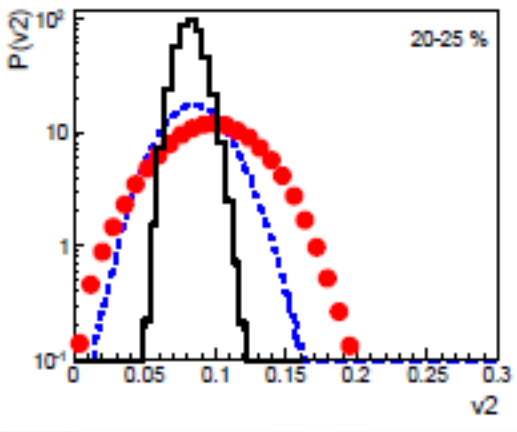

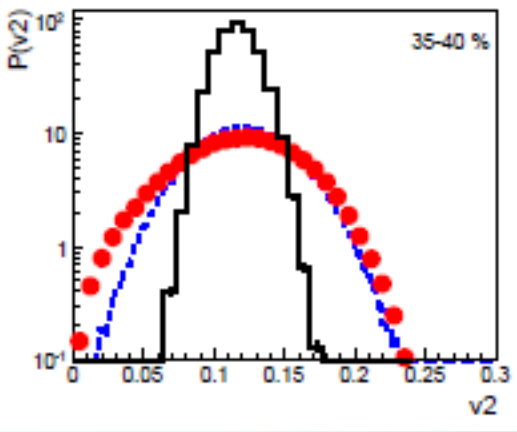

Normally smeared ε

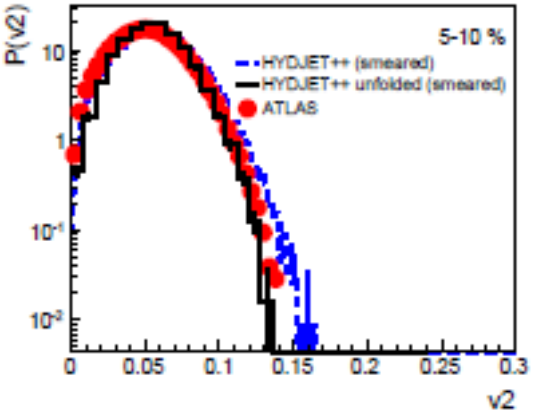

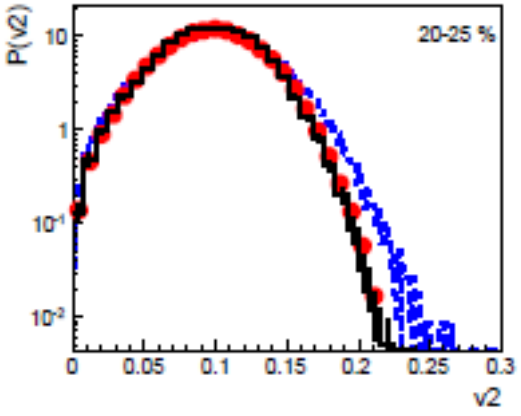

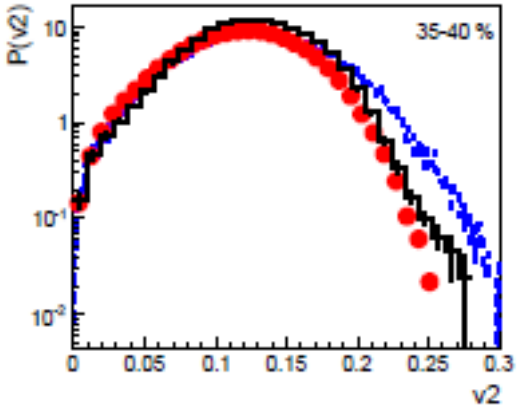

L. Bravina et al., EPJC 75 (2015) 588

Note: the smearing width for ε is optimized at one centrality and then fixed for other centrality bins

Fluctuations of triangular flow in the model

Unsmeared parameter ε_3

Pb+Pb @ 2.76 ATeV

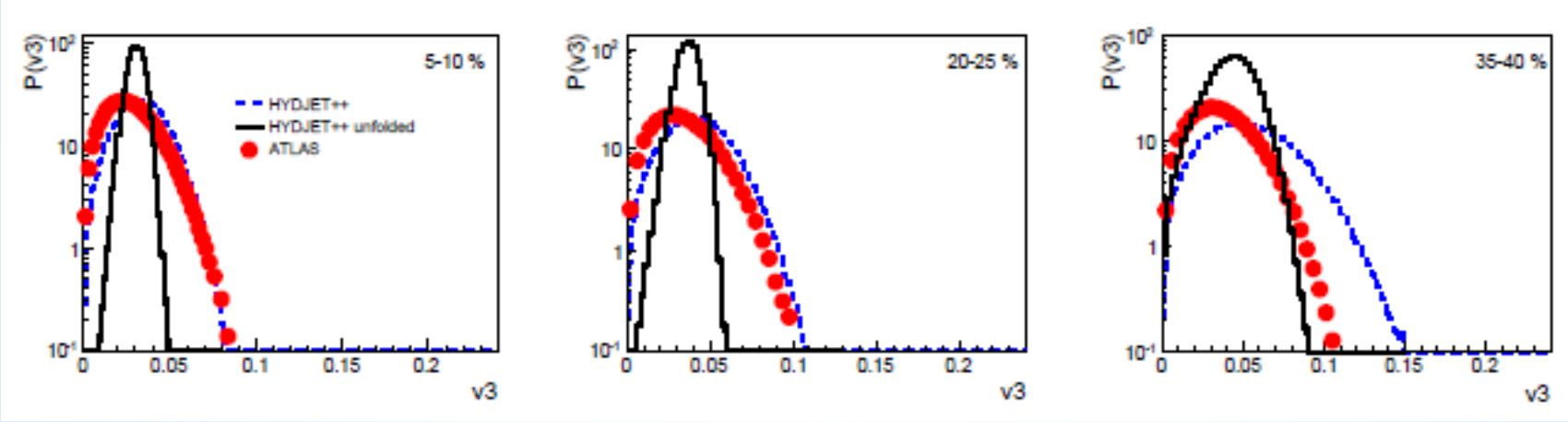

Normally smeared ε_3

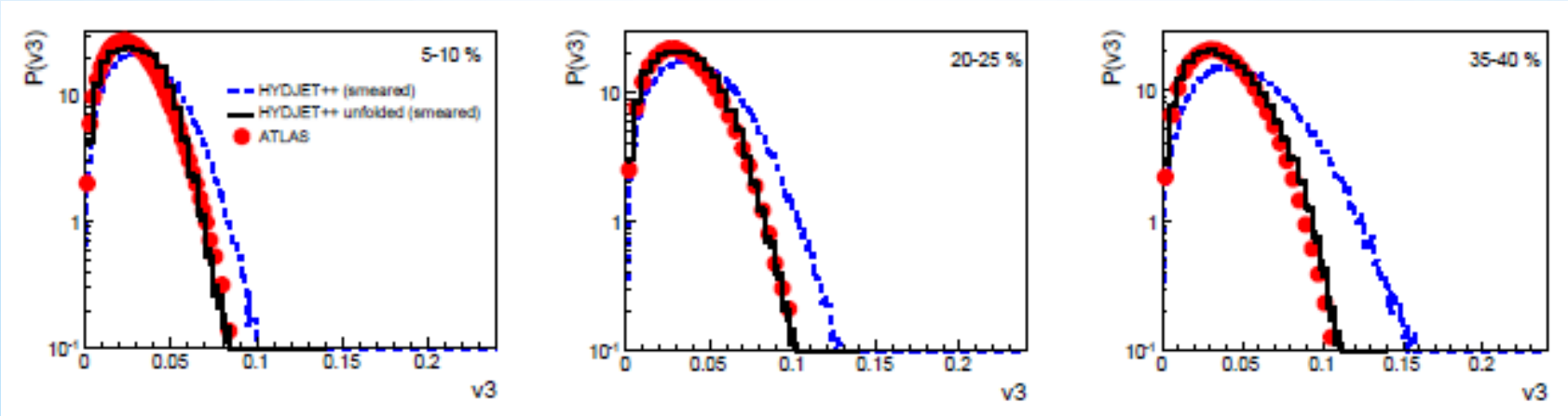

L. Bravina et al., EPJC 75 (2015) 588

Note: the smearing width for ε_3 is optimized at one centrality and then fixed for other centrality bins

IV. Femtoscopic correlations

QS symmetrization of production amplitude

→ *momentum correlations of identical particles are sensitive to space-time structure of the source*

KP'71-75

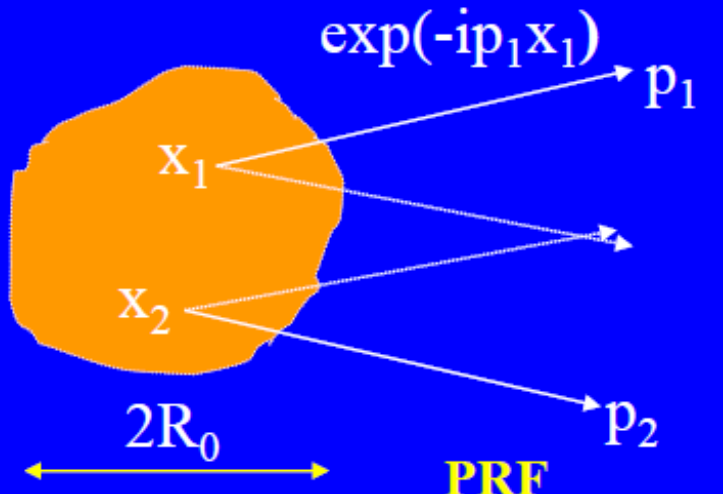

$q = p_1 - p_2$; $\Delta x = x_1 - x_2$

total pair spin

$CF = 1 + (-1)^S \langle \cos q\Delta x \rangle$

Grassberger'77
Lednicky'78

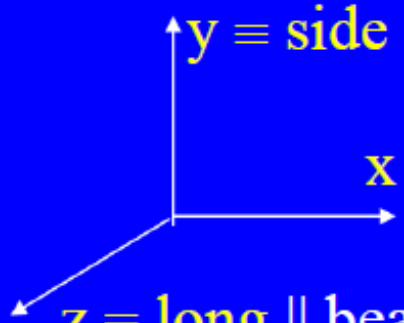

$\langle \cos q\Delta x \rangle = 1 - \frac{1}{2}\langle (q\Delta x)^2 \rangle + .. \approx \exp(-R_x^2 q_x^2 - R_y^2 q_y^2 - R_z^2 q_z^2 - 2R_{xz}^2 q_x q_z)$

Femtoscopy or Interferometry radii:

$R_x^2 = \frac{1}{2} \langle (\Delta x - v_x \Delta t)^2 \rangle$, $R_y^2 = \frac{1}{2} \langle (\Delta y)^2 \rangle$, $R_z^2 = \frac{1}{2} \langle (\Delta z - v_z \Delta t)^2 \rangle$

Probing source dynamics - expansion

Dispersion of emitter velocities & limited emission momenta (**T**) ⇒
x-p correlation: interference dominated by pions from nearby emitters

→ **Interference probes only a part of the source**

→ **Interferometry radii decrease with pair velocity**

Resonances GKP'71
Strings Bowler'85 ..
Hydro Pratt'84,86
Kolehmainen, Gyulassy'86
Makhlin-Sinyukov'87
Bertch, Gong, Tohyama'88
Hama, Padula'88
Pratt, Csörgö, Zimanyi'90
Mayer, Schnedermann, Heinz'92
.....

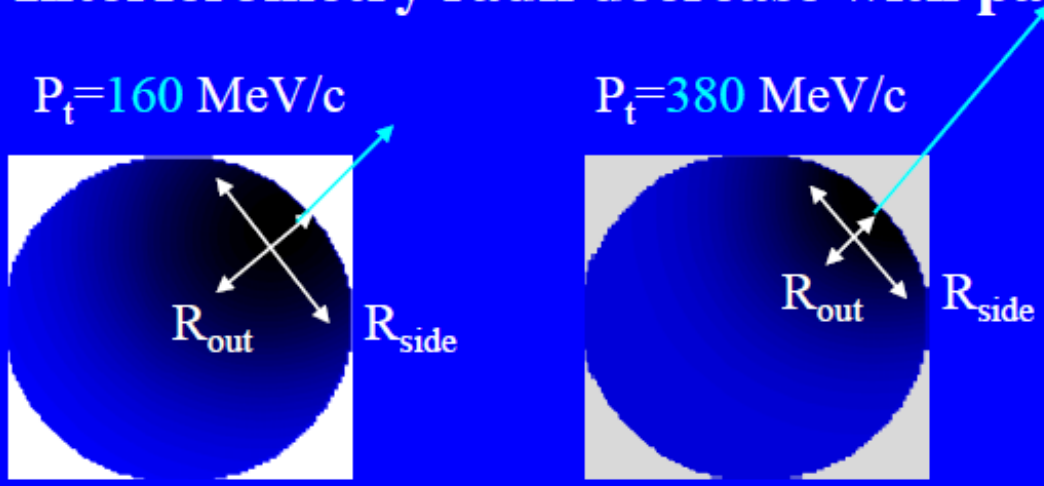

Collective transverse flow β^F → $R_{side} \approx R/(1+m_t \beta^{F2}/T)^{½}$

in LCMS: 1

Longitudinal boost invariant expansion during proper freeze-out (evolution) time τ → $R_{long} \approx (T/m_t)^{½}\tau/\widetilde{\cosh y}$

Expected evolution of HI collision vs RHIC data

Bass'02

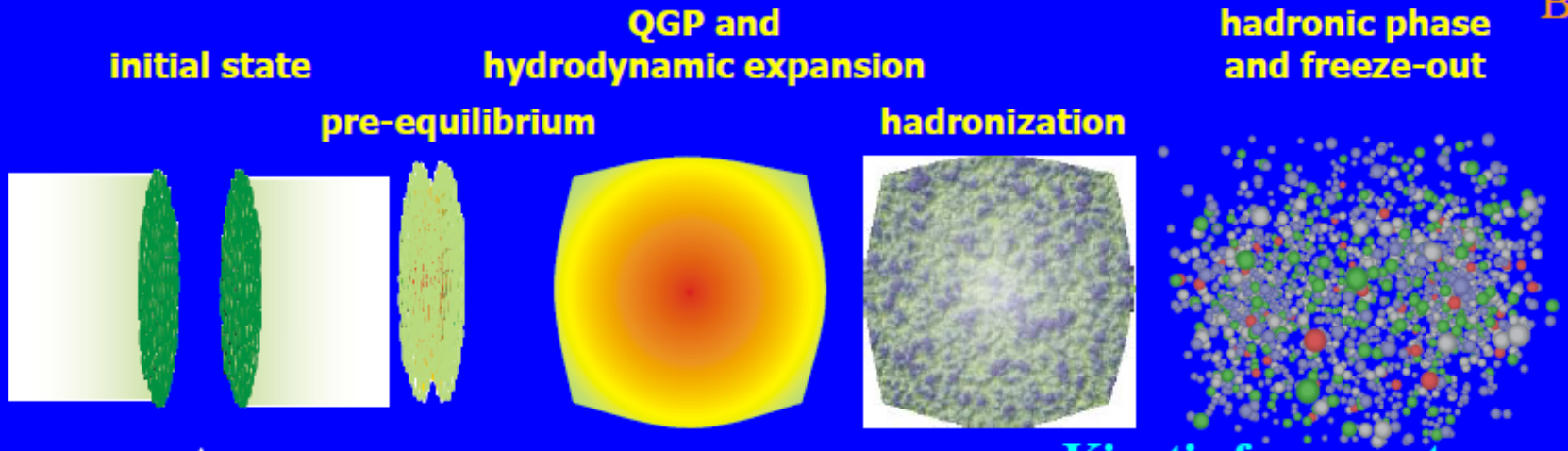

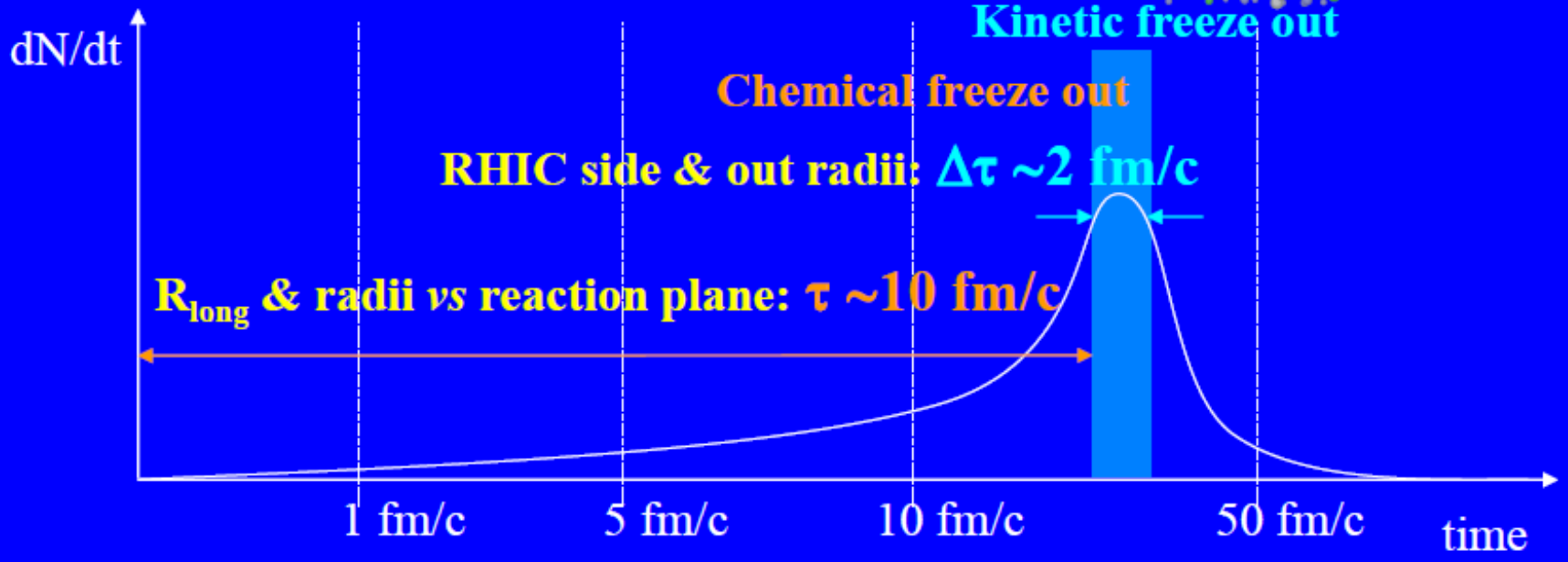

V. Geometric and dynamical anisotropy: consequences for flow and radii

Results: Phenix paper

Angular dependence of radii fit with:

$$R_\mu^2 = R_0^2 + 2\sum_{n=m,2m} R_{\mu,n}^2 \cos\left[n\left(\phi - \Psi_m\right)\right] \quad (\mu = s,o,l)$$

$$R_\mu^2 = 2\sum_{n=m,2m} R_{\mu,n}^2 \sin\left[n\left(\phi - \Psi_m\right)\right] \quad (\mu = os)$$

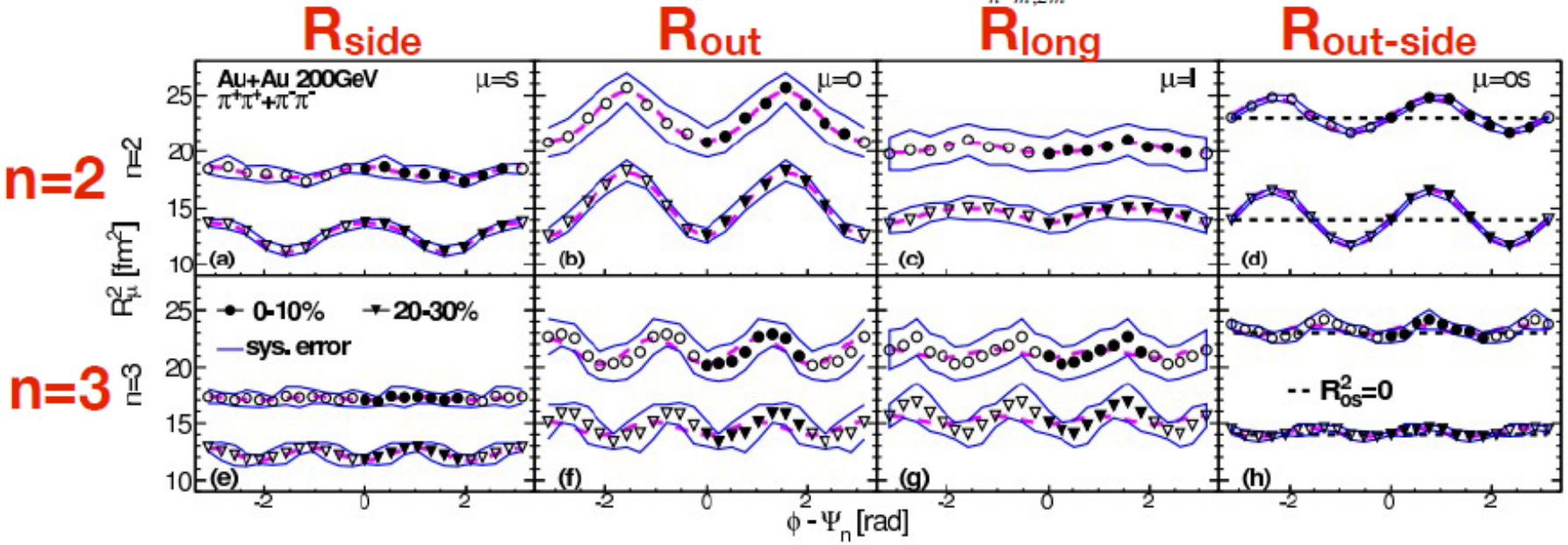

FIG. 1: (Color online) The azimuthal dependence of R_s^2, R_o^2, R_l^2, and R_{os}^2 for charged pions in $0.2 < k_T < 2.0$ GeV/c with respect to 2nd (a-d) and 3rd-order (e-h) event plane in Au+Au collisions at $\sqrt{s_{NN}} = 200$ GeV. The R_{os}^2 is plotted relative to dashed lines representing $R_{os}^2 = 0$. The filled symbols show the extracted HBT radii and the open symbols are reflected by symmetry around $\phi - \Psi_n = 0$. Bands of two thin lines show the systematic uncertainties and dashed lines show the fit lines by Eq. (3).

$0-10\%: R_S^2$ shows a weak oscillation for Ψ_2, Ψ_3

R_O^2 shows a strong oscillation for Ψ_2, Ψ_3

$20-30\%: R_S^2$ & R_O^2 shows opposite oscillation for Ψ_2

R_S^2 shows a weak oscillation with same sign for Ψ_3

RHIC

WAYNE STATE UNIVERSITY

Summary 1: Gaussian Toy Model

Plumberg, Chun, & Heinz Phys. Rev. C **88**, 044914 (2013)

- Do we understand the third order HBT oscillation?

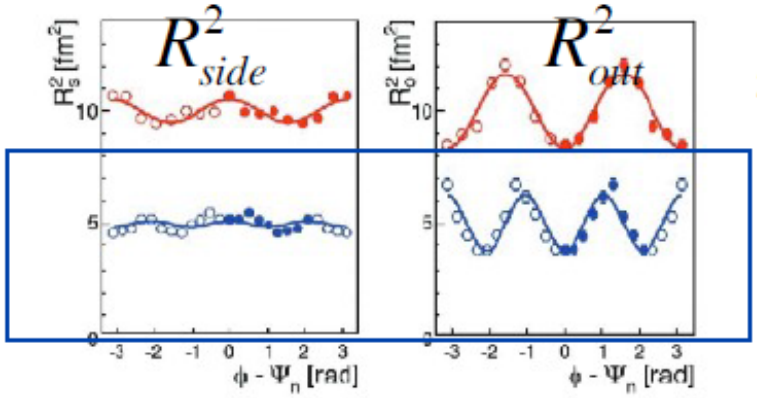

2nd order

3rd order

FIG. 2. (Color online) Second- and third-order oscillations of R_s^2 and R_o^2 measured by the PHENIX Collaboration in central (0%–10%) 200 A GeV Au + Au collisions [13]. For better visibility, the average values $R^2_{s,0}$, $R^2_{o,0}$ of the two radius parameters were set by hand to 5 and 10 fm^2, respectively, when plotting the third- and second-order oscillations.

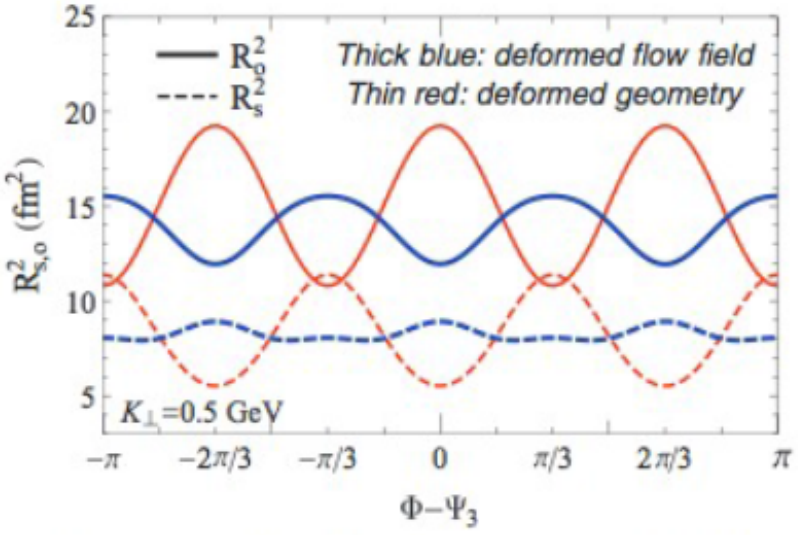

FIG. 3. (Color online) Triangular oscillations of R_s^2 (dashed) and R_o^2 (solid) for pion pairs with momentum $K_\perp = 0.5$ GeV, as a function of emission angle Φ relative to the triangular flow direction Ψ_3. Shown are results for two model scenarios: A deformed flow field ($\bar{v}_3 = 0.25$) in a spatially isotropic ($\bar{\epsilon}_3 = 0$) density distribution (thick blue lines), and a source with triangular geometric deformation ($\bar{\epsilon}_3 = 0.25$) expanding with radially symmetric ($\bar{v}_3 = 0$) flow (thin red lines). For the two scenarios the oscillations of both R_s^2 and R_o^2 are seen to be out of phase by $\pi/3$.

Deformed flow field simulation (blue) is in agreement with data

Deformed geometry field simulation (red) does not follow data

This compliments PHENIX figure 3 & MC simulation

Summary 1: Gaussian Toy Model

Plumberg, Chun, & Heinz Phys. Rev. C **88**, 044914 (2013)

Do we understand $2R^2_{s,3}/R^2_{s,0}$?

deformed geometry

deformed flow

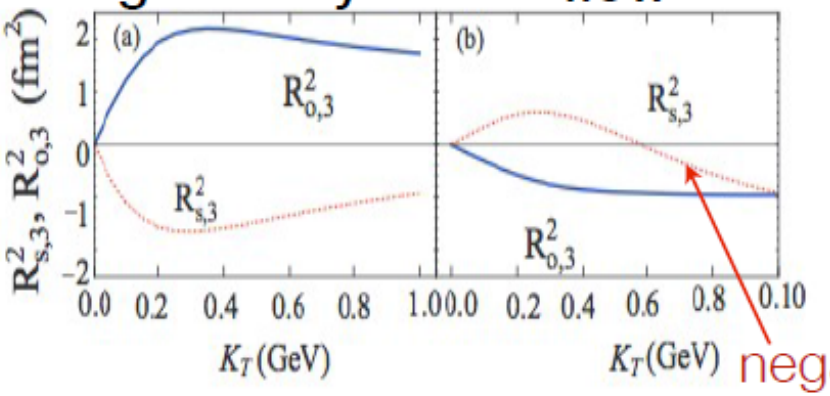

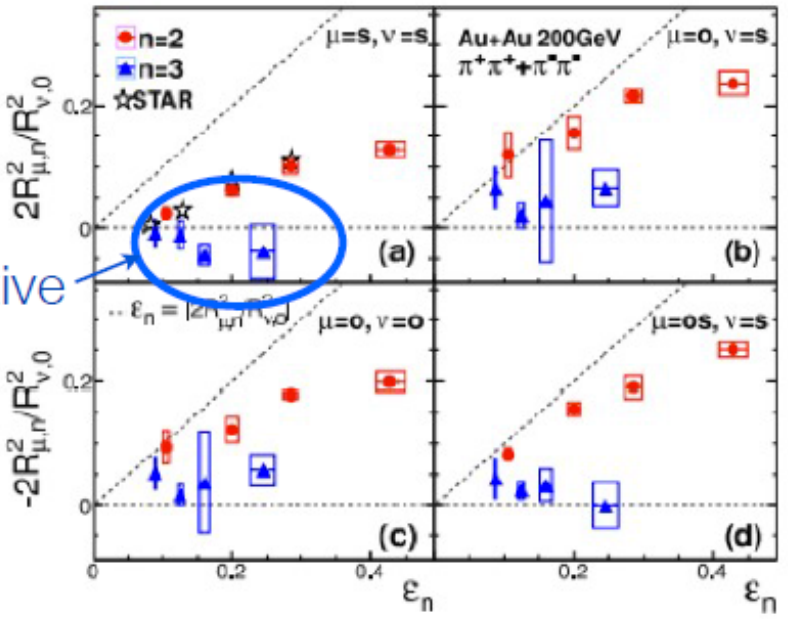

$R^2_{s,3}$ goes negative for the deformed flow case, this may be why $2R^2_{s,3}/R^2_{s,0}$ may be less than equal to zero.

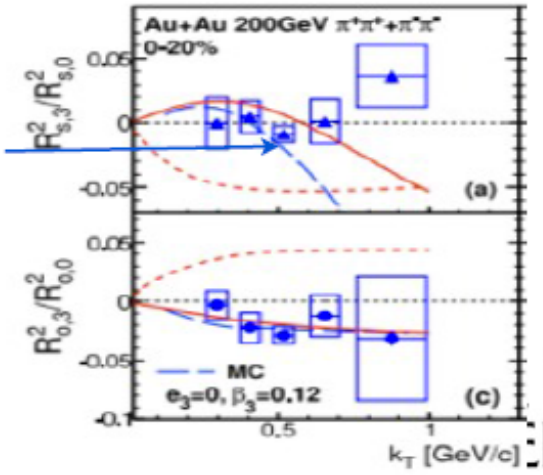

Azimuthally sensitive HBT radii w.r.t. Ψ_2

- k_T:0.2-2.0(GeV/c)
- Ψ_2 is measured via FMD A+C

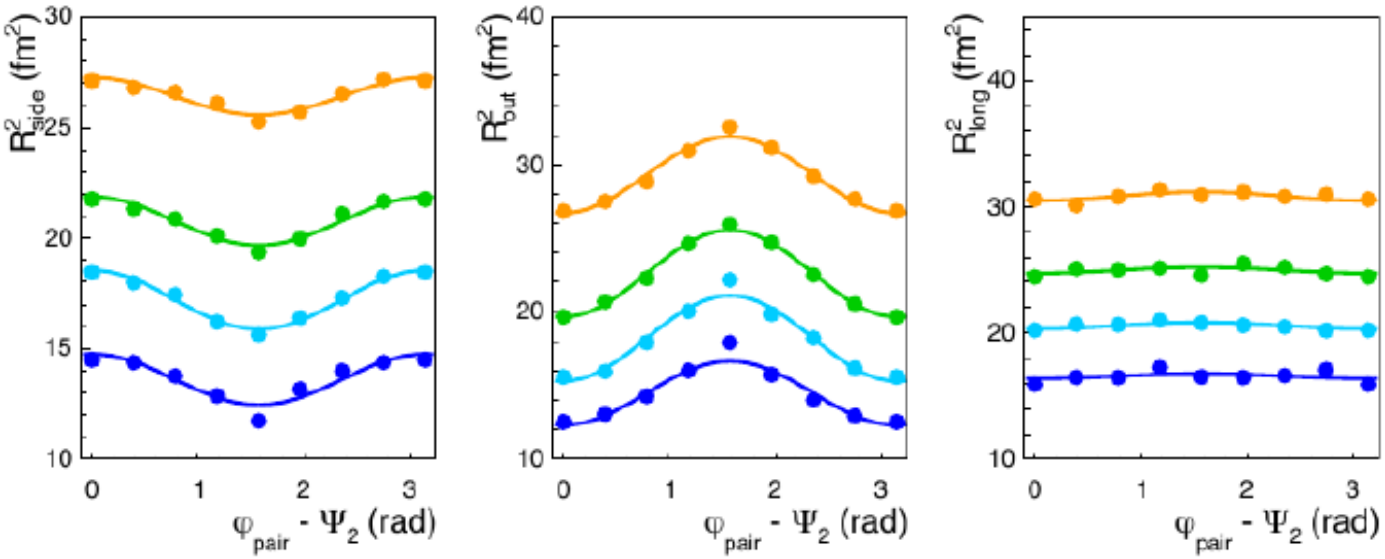

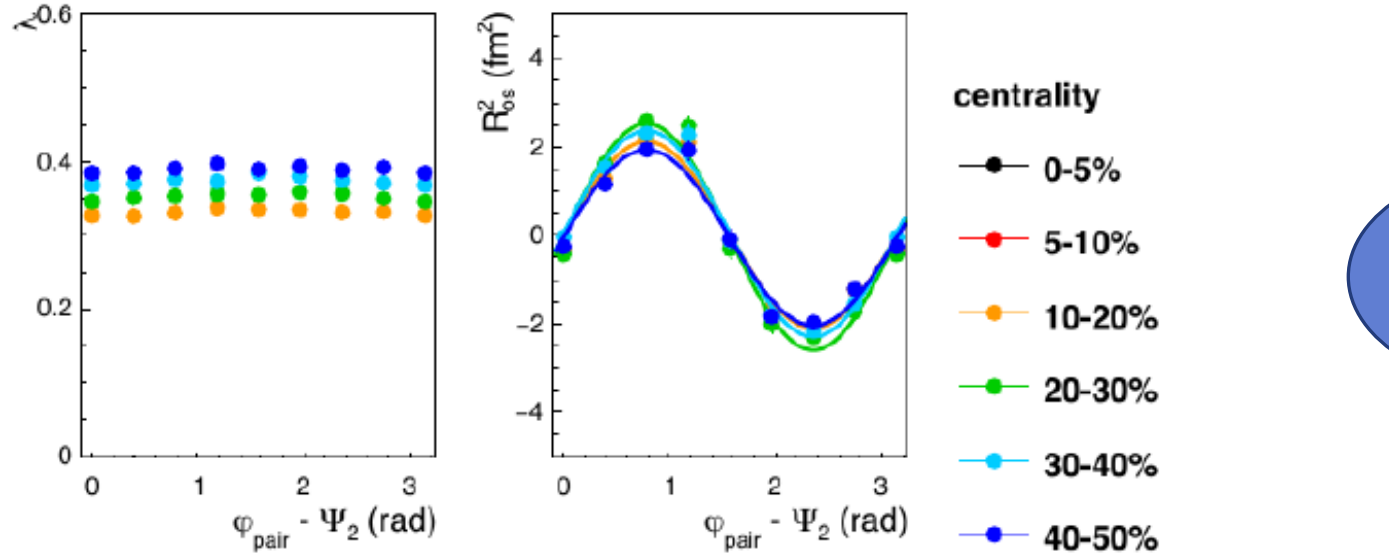

LHC

Azimuthally sensitive HBT radii w.r.t. Ψ_3

- **kT:0.2-2.0(GeV/c)**
  - Ψ_3 **is measured via FMD A+C**

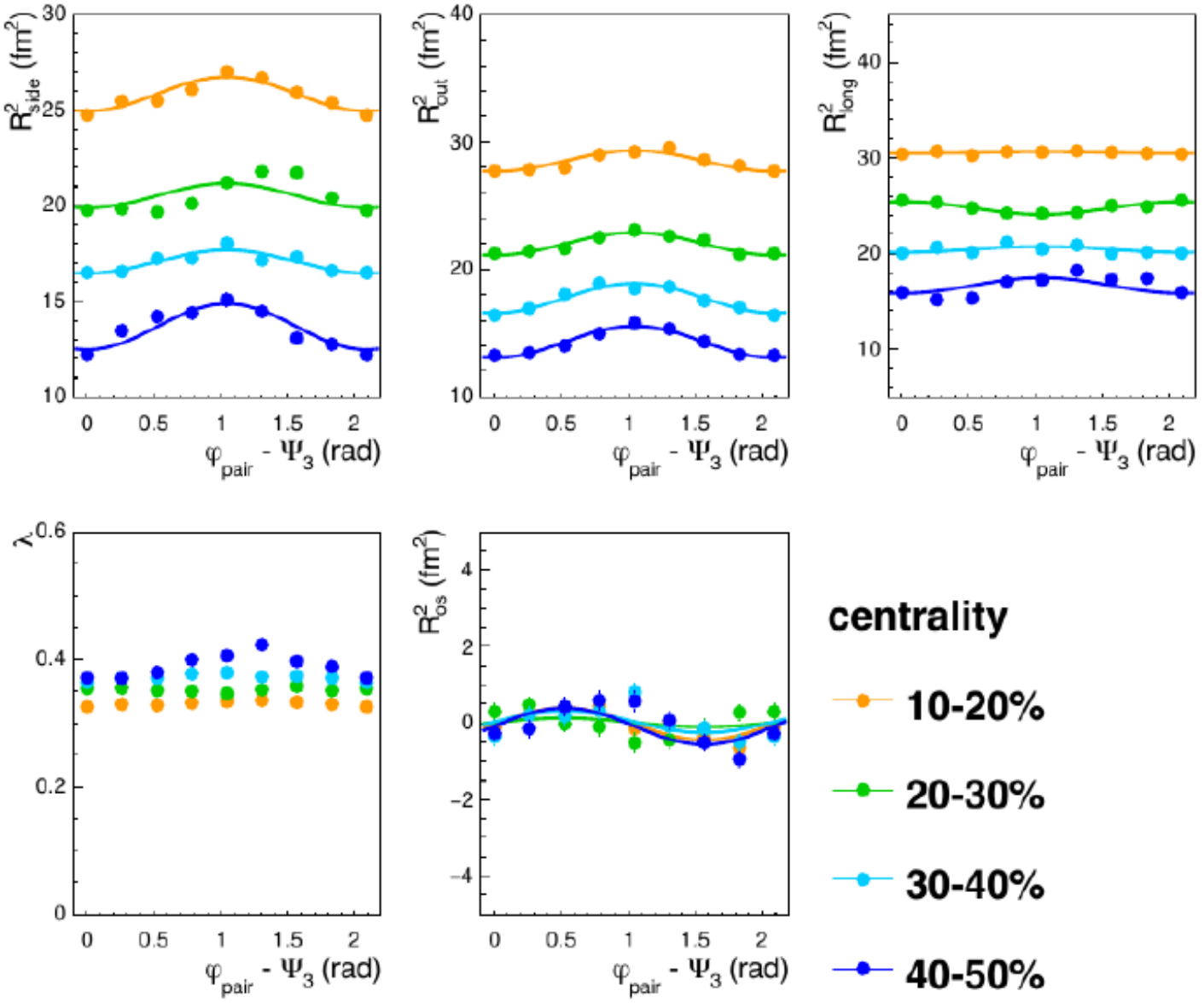

VI. Simultaneous description of the flow and HBT radii

M.Lisa, U.Heinz, U.Wiedemann, PLB 480 (2000) 287
M.Csanad, B.Tomasik, T.Csorgo, EPJA 37 (2008) 111
C.Plumberg, C.Shen, U.Heinz, PRC 88 (2013) 044914
S.Lökös et al., EPJA 52 (2016) 311
J.Cimerman et al., EPJA 53(2017) 161
L. Bravina et al., EPJA 53 (2017) 219
…

Spatial vs Dynamical Anisotropy

L. Bravina et al., Eur.Phys.J. A53 (2017) 219 / arXiv: 1709.08602 [hep-ph]

Elliptic flow and radii oscillations w.r.t. Ψ2 plane

Pb+Pb @ 2.76 TeV

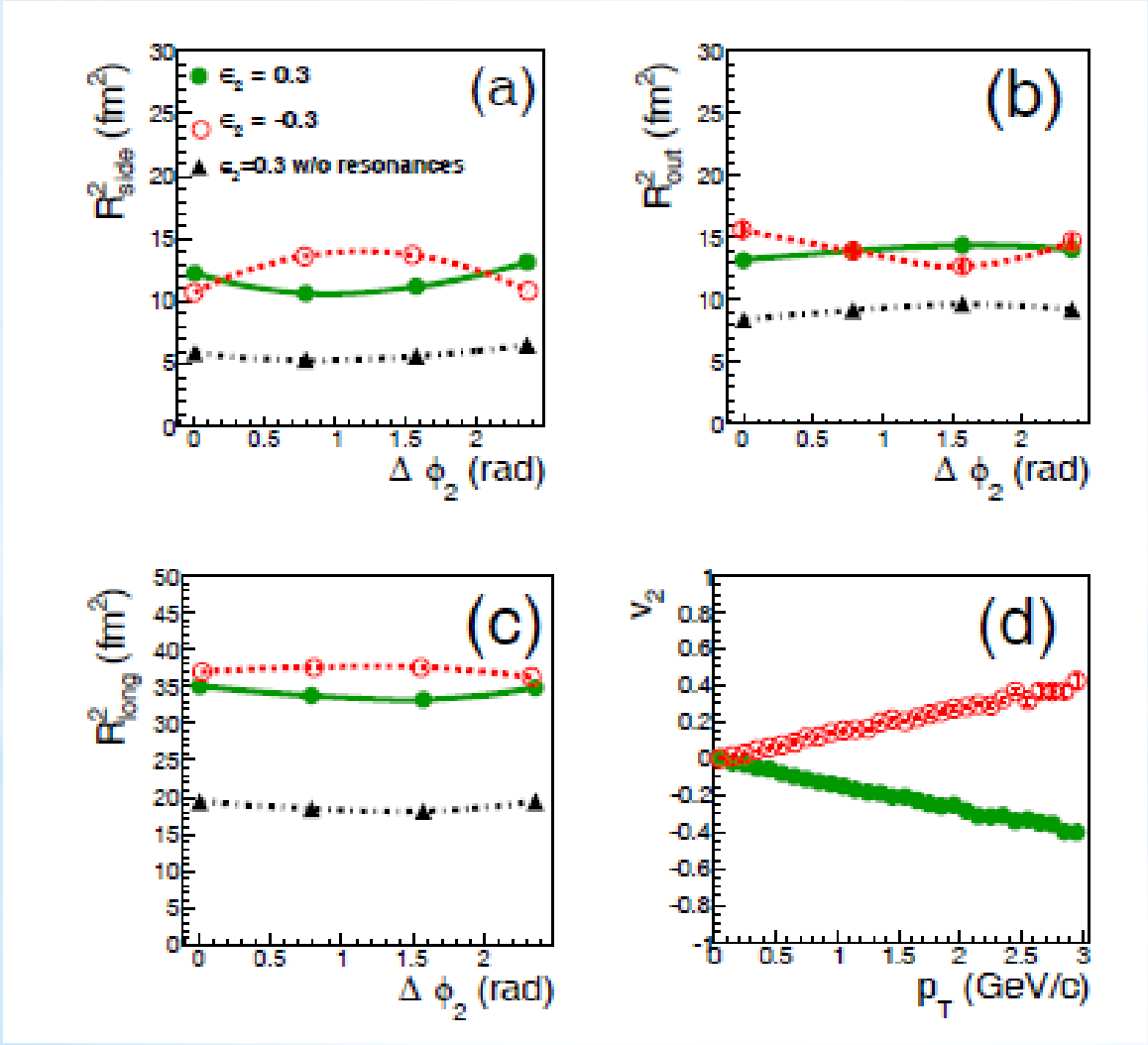

$\varepsilon_2 = \pm 0.3$

Other anisotropy parameters are zero (only spatial anisotropy).

Either flow or radii oscillations !?

Spatial vs Dynamical Anisotropy

Elliptic flow and radii oscillations w.r.t. Ψ2 plane

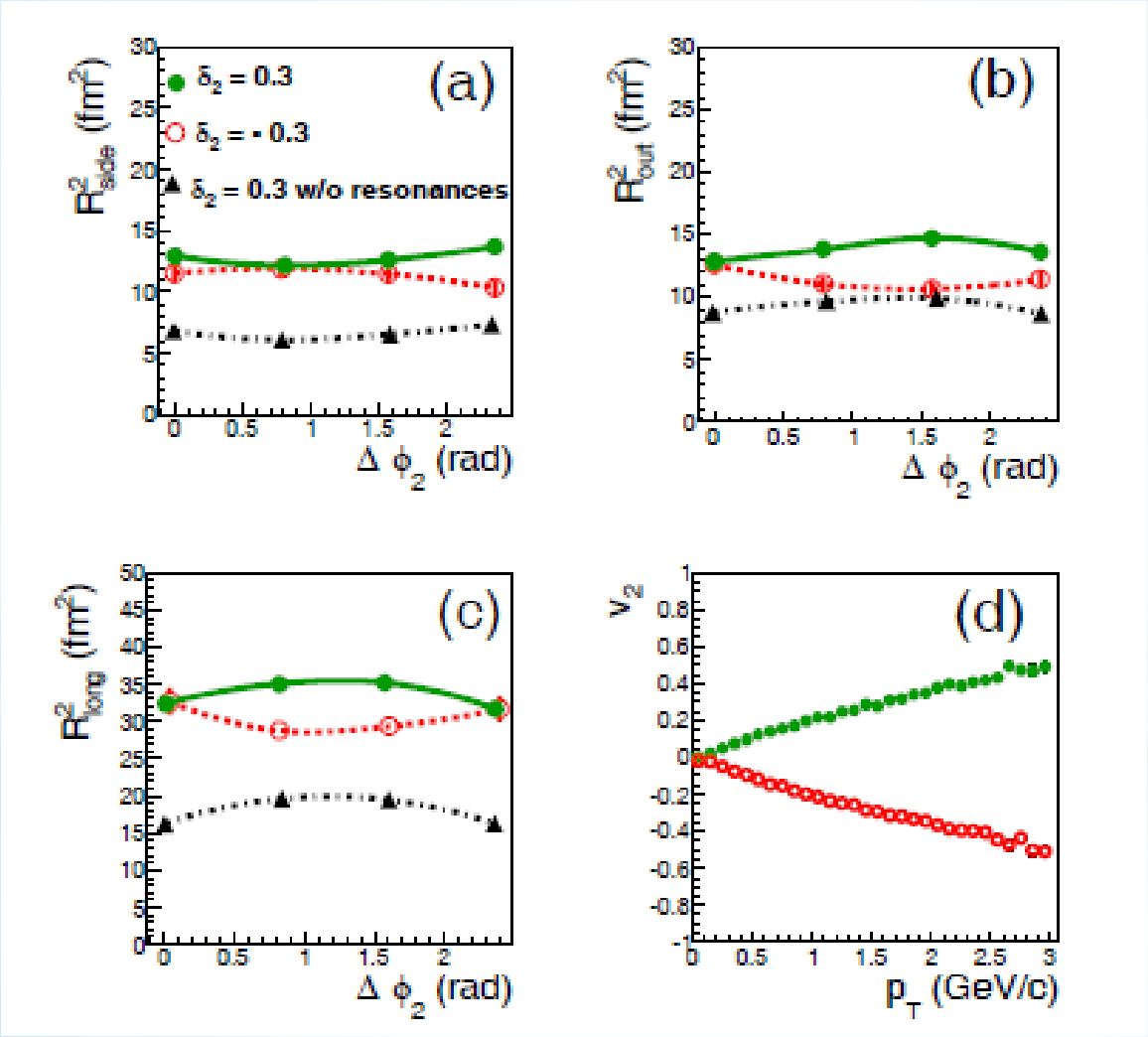

$\delta_2 = \pm 0.3$

Other anisotropy parameters are zero (only dynamical anisotropy).

Correct v_2 and oscillation phases for $\delta_2 > 0$

Spatial vs Dynamical Anisotropy

Triangular flow and radii oscillations w.r.t. Ψ_3 plane

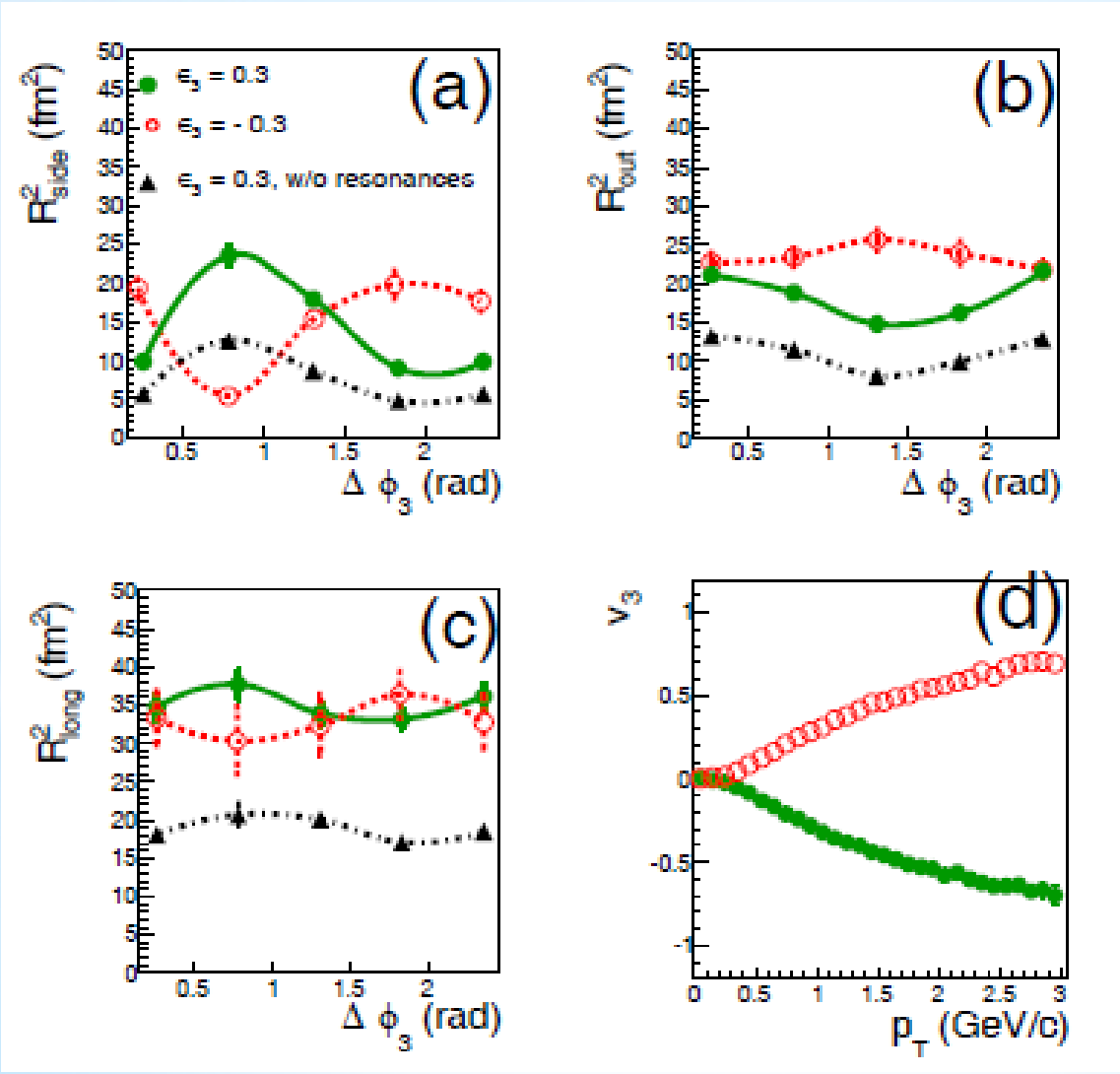

$\varepsilon_3 = \pm 0.3$

Other anisotropy parameters are zero (only spatial anisotropy). **Again, either flow or radii oscillations are reproduced**

Spatial vs Dynamical Anisotropy

Triangular flow and radii oscillations w.r.t. Ψ_3 plane

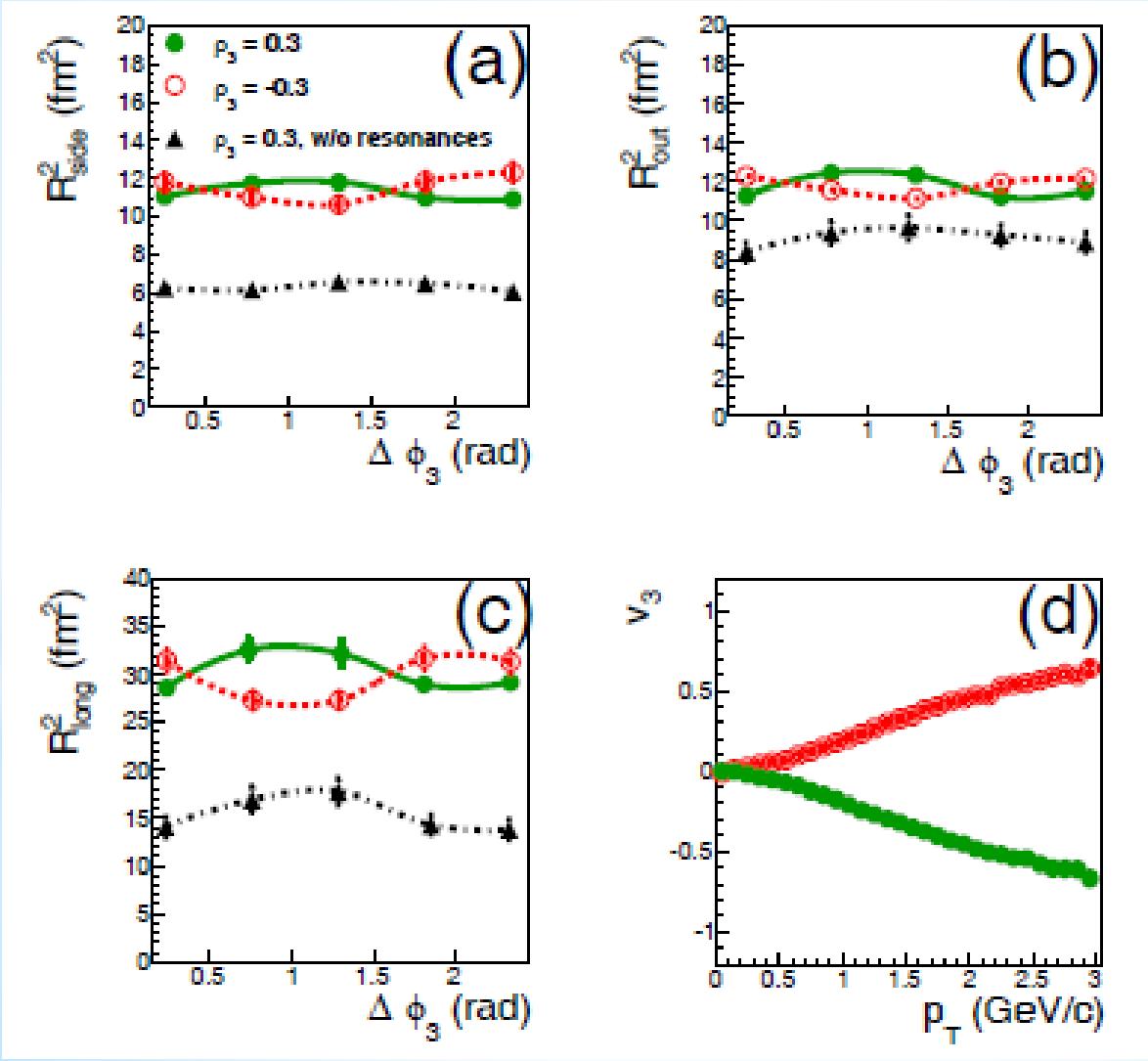

$\rho_3 = \pm 0.3$

Other anisotropy parameters are zero (only dynamical anisotropy).

Correct v_3 and oscillation phases for $\rho_3 > 0$

Spatial vs Dynamical Anisotropy. Influence of resonance decays

Spatial

Dynamical

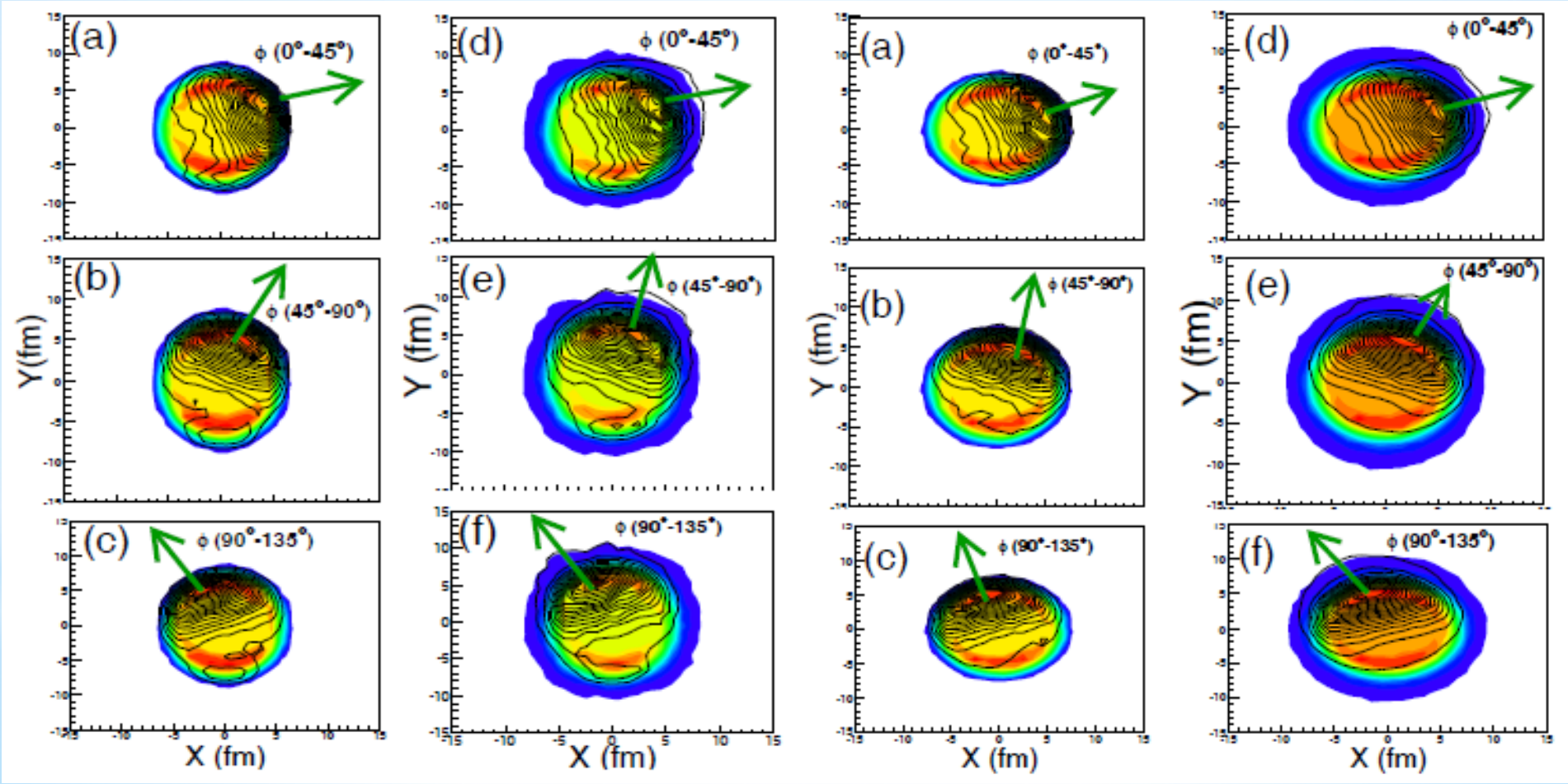

Elliptic anisotropy

Spatial vs Dynamical Anisotropy. Influence of resonance decays

Spatial

Dynamical

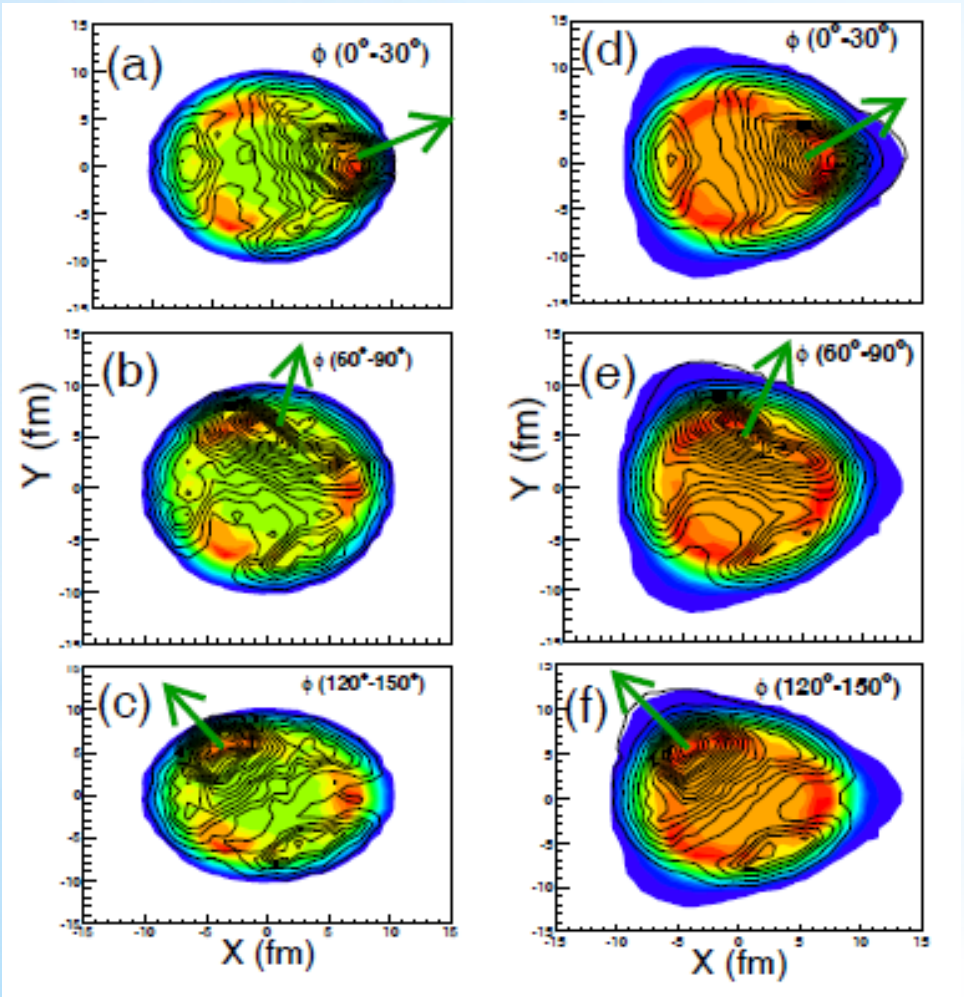

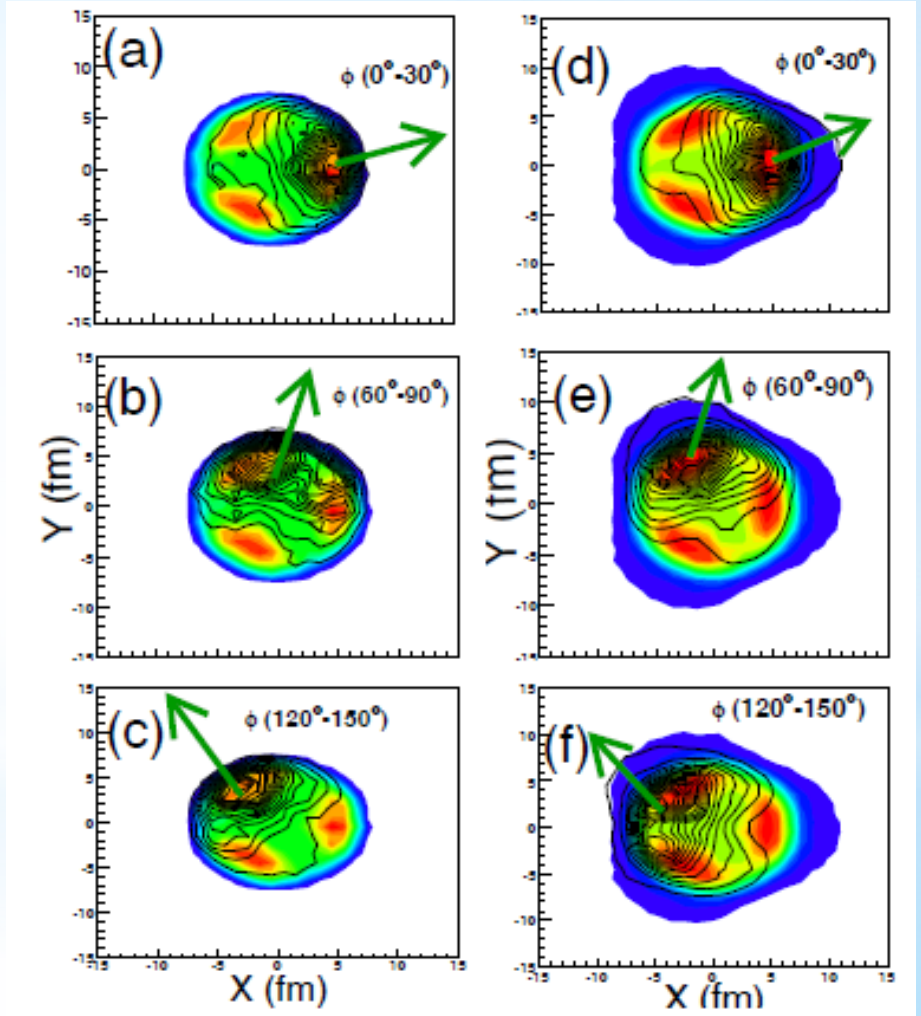

Triangular anisotropy

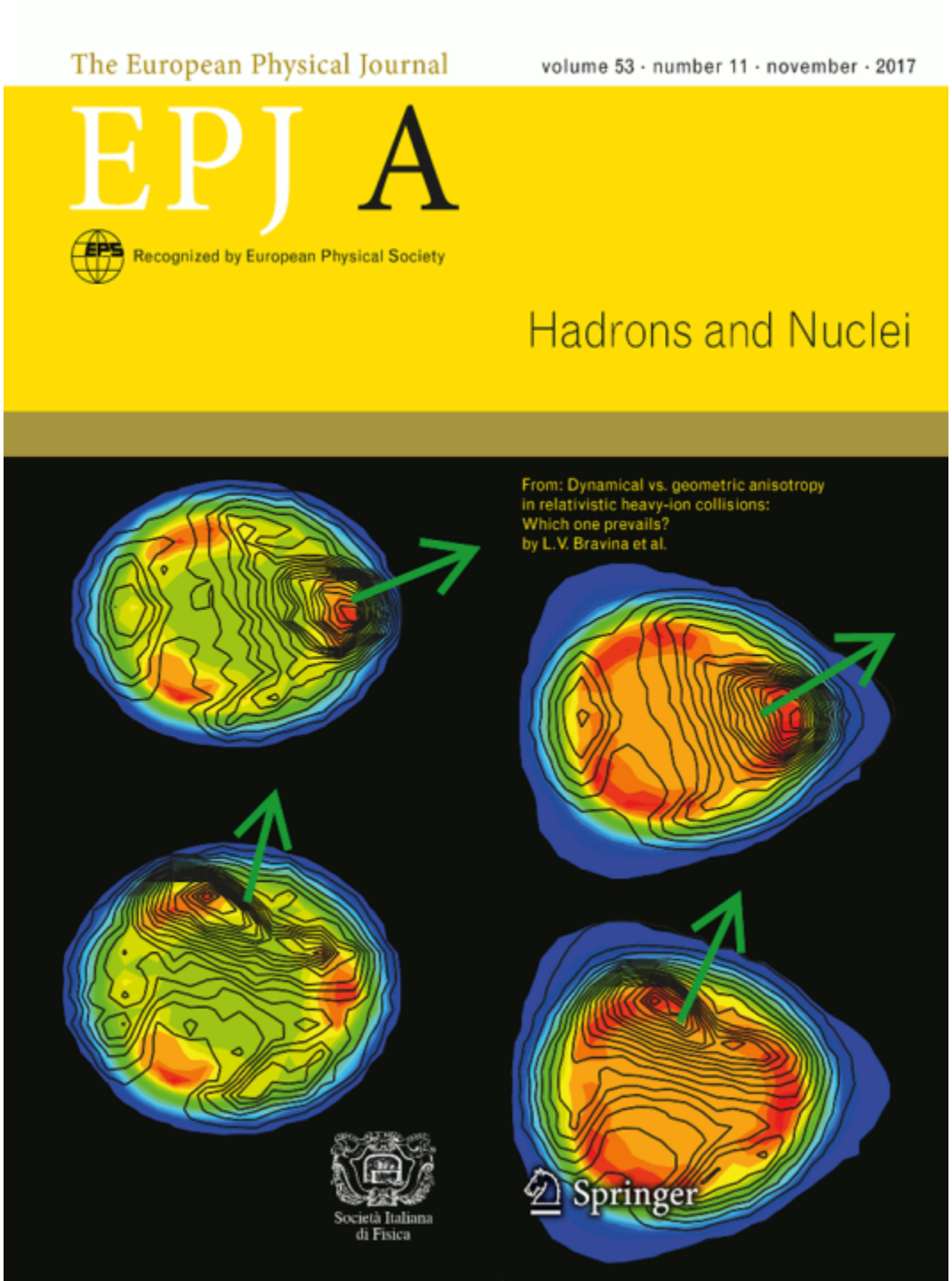

L.V. Bravina,
I.P. Lokhtin,
L.V. Malinina,
S.V. Petrushanko,
A.M. Snigirev,
E.E. Zabrodin,
”Dynamical vs. geometric anisotropy in relativistic heavy-ion collisions: Which one prevails?”,
Eur. Phys. J. A 53 (2017) 219.

CONCLUSIONS

Second- and third-order oscillations of the femtoscopic radii in Pb+Pb collisions at 2.76 TeV were studied within the HYDJET++ model together with the differential elliptic and triangular flow. Our study indicates that

- ***Elliptic or triangular spatial anisotropy alone cannot reproduce simultaneously the correct phase of the radii oscillations and the correct sign of the corresponding flow harmonics***
- ***Dynamical flow anisotropy provides correct qualitative description of both P_T –dependence of v_2 and v_3 and the phases of the femtoscopic radii oscillations***
- ***Decays of resonances provide significant increase of the emitting areas and make the radii oscillations more pronounced***
- ***However, they do not change the phases of the oscillations***
- ***Both spatial and dynamical anisotropy is needed for the quantitative description of both signals.***

Back-up Slides

Suppression factor of inclusive jets vs P_T in PYQUEN at LHC

I.P. Lokhtin, A.A. Alkin, A.M. Snigirev, Eur.Phys. J. C (2015) 75

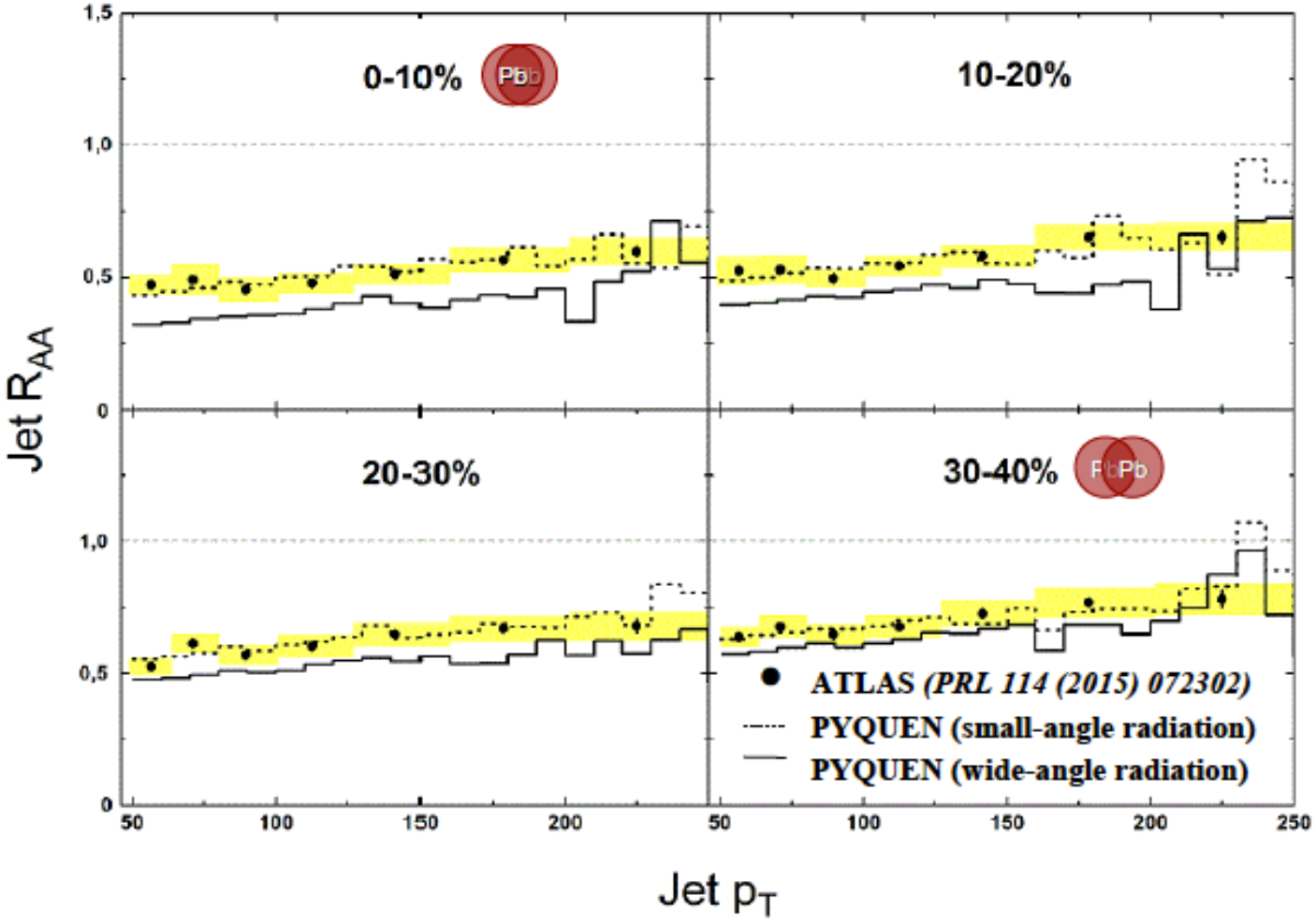

PYQUEN simulation results for R_{AA} are close to the data within statistical and systematic experimental uncertainties.

Suppression factor of b-jets vs. p_T in CMS and PYQUEN

I.P. Lokhtin, A.A. Alkin, A.M. Snigirev, Eur.Phys. J. C (2015) 75

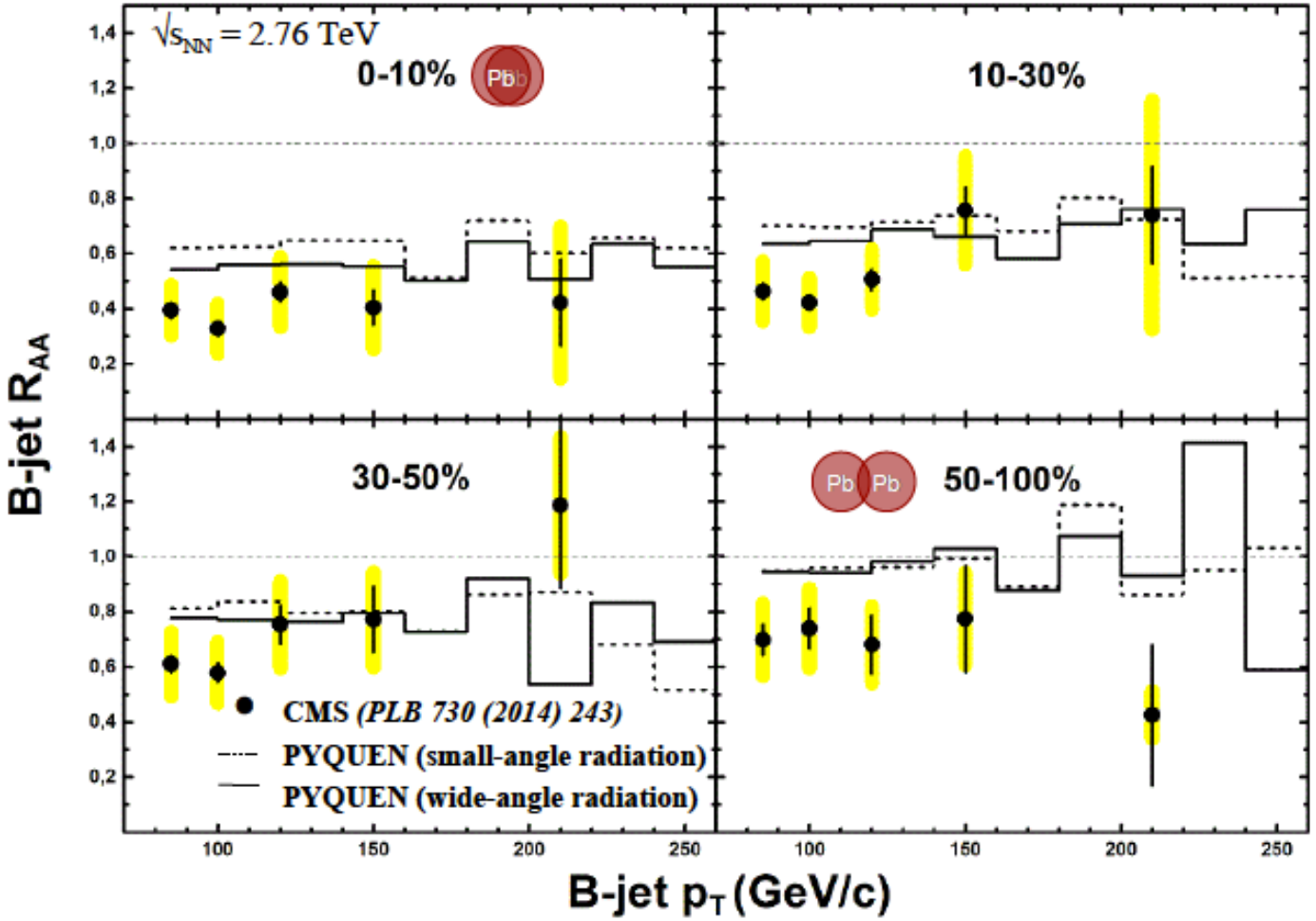

Reproduced well by PYQUEN

Jet shapes
PYQUEN vs. CMS data

$$\rho(r) \sim \frac{1}{\delta r}\frac{1}{N_{\text{jet}}}\sum_{\text{jets}}\frac{p_{\text{T}}(r-\delta r/2, r+\delta r/2)}{p_{\text{T}}^{\text{jet}}}$$

二十五

I.P. Lokhtin, A.A. Alkin, A.M. Snigirev, Eur.Phys. J. C (2015) 75

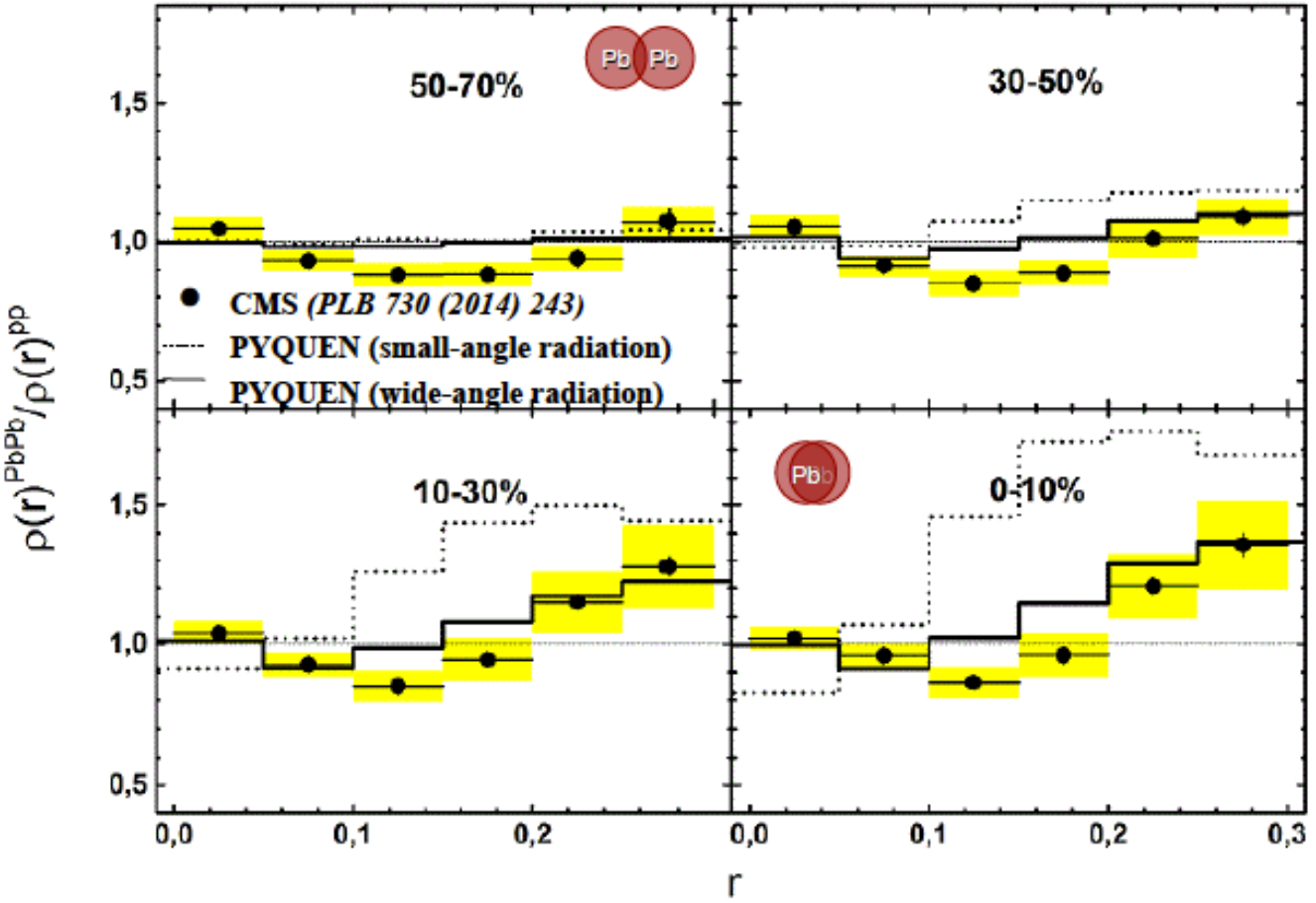

The modification of radial jet profile (E_T^{jet}>100 GeV, R=0.3): excess at large radii; suppression at intermediate radii; core is unchanged. Reproduced well by PYQUEN with wide-angle radiative + collisional partonic energy loss.

Jet fragmentation function PYQUEN vs. CMS data

$$\xi = -\ln z = -\ln \frac{p_T^{track}}{p_T^{jet}}$$

I.P. Lokhtin, A.A. Alkin, A.M. Snigirev, Eur.Phys. J. C (2015) 75

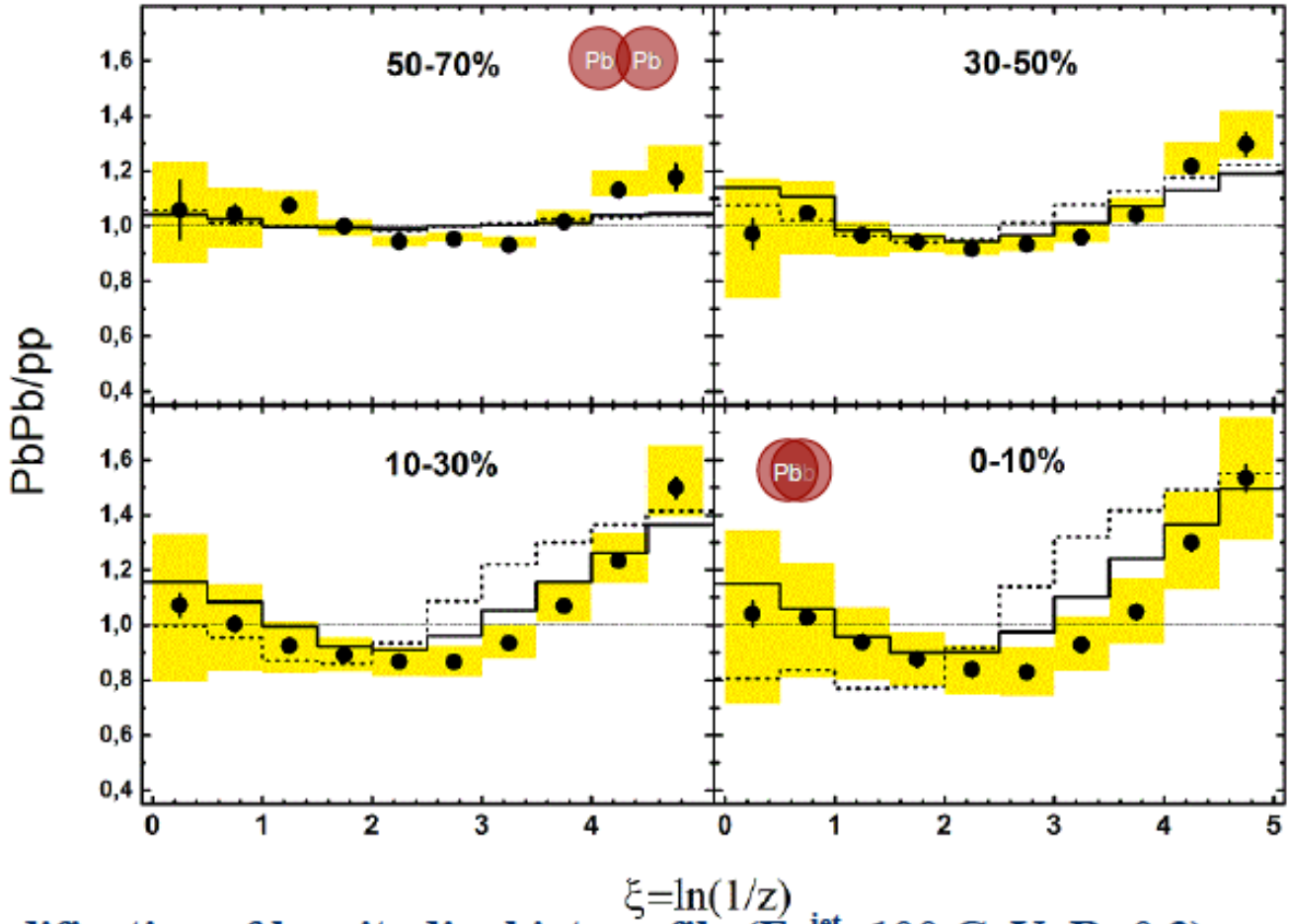

The modification of longitudinal jet profile (E_T^{jet}>100 GeV, R=0.3): excess at low p_T; suppression at intermediate p_T; high p_T is slightly enhanced. Reproduced well by PYQUEN with wide-angle radiative + collisional partonic energy loss.

Thermal production

- Hadrons are produced on the freeze-out hypersurface with particle density ρ and effective volume V_{eff}. Multiplicities are defined with T^{ch} for stable hadrons and resonances:

$$\overline{N_i} = \rho_i(T, \mu_i) V_{eff}$$

Mean multiplicity

$$P(N_i) = \exp(-\overline{N_i}) \frac{(\overline{N_i})^{N_i}}{N_i!}$$

EbE distribution

- Momentum distribution is defined with T^{th}.

$$f_i^{eq}(p^{*0}, T^{th}, \mu_i, \gamma_s) = \frac{g_i}{\gamma_s^{-n_i^s} \exp([p^{*0} - \mu_i]/T^{th}) \pm 1}$$

Momentum distribution function in the fluid element rest frame

- Decay kinematics is taken into account.

- The final hadron spectrum are given by the superposition of thermal distribution and collective flow of fireball liquid assuming Bjorken's scaling.

Monte-Carlo simulation of hard component (including nuclear shadowing) in HYDJET/HYDJET++

- Calculating the number of hard NN sub-collisions Njet (b, Ptmin, $\sqrt{s}$) with Pt>Ptmin around its mean value according to the binomial distribution.
- Selecting the type (for each of Njet) of hard NN sub-collisions (pp, np or nn) depending on number of protons (Z) and neutrons (A-Z) in nucleus A according to the formula: $Z=A/(1.98+0.015A^{2/3})$.
- Generating the hard component by calling PYQUEN njet times.
- Correcting the PDF in nucleus by the accepting/rejecting procedure for each of Njet hard NN sub-collisions: comparision of random number generated uniformly in the interval [0,1] with shadowing factor $S(r1,r2,x1,x2,Q2) \leq 1$ taken from the adapted impact parameter dependent parameterization based on Glauber-Gribov theory (*K.Tywoniuk et al., Phys. Lett. B 657 (2007) 170*).

p_T-spectra of identified hadrons

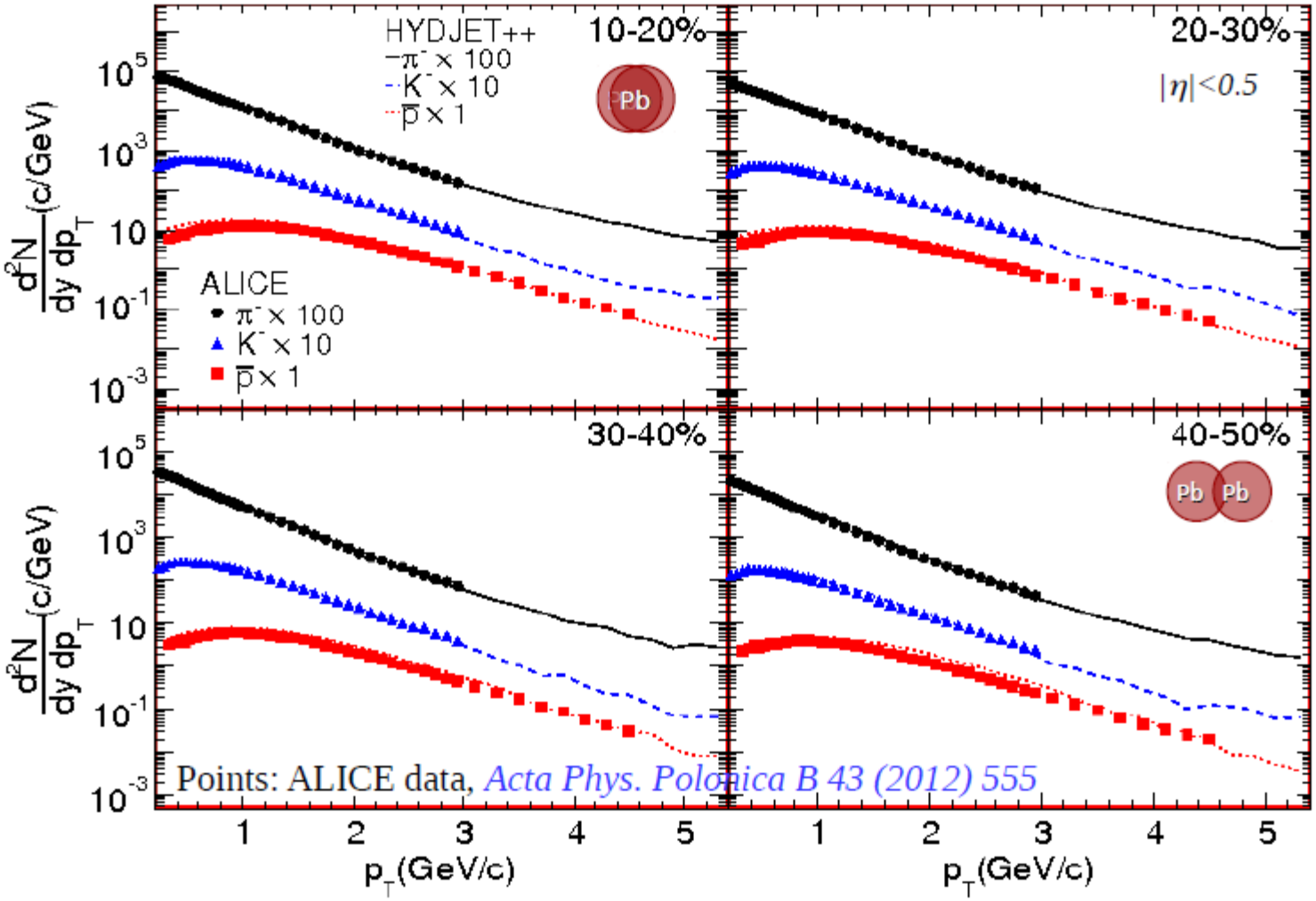

HYDJET++ reproduces p_T-spectrum of pions, kaons and (anti-)protons.